

Interaction of tearing modes with external structures in cylindrical geometry (plasma)

This content has been downloaded from IOPscience. Please scroll down to see the full text.

1993 Nucl. Fusion 33 1049

(<http://iopscience.iop.org/0029-5515/33/7/108>)

View [the table of contents for this issue](#), or go to the [journal homepage](#) for more

Download details:

IP Address: 128.62.18.33

This content was downloaded on 12/03/2015 at 15:22

Please note that [terms and conditions apply](#).

INTERACTION OF TEARING MODES WITH EXTERNAL STRUCTURES IN CYLINDRICAL GEOMETRY

R. FITZPATRICK

UKAEA/Euratom Fusion Association,
AEA Fusion,
Culham Laboratory,
Abingdon, Oxfordshire,
United Kingdom

ABSTRACT. A basic theoretical framework is developed for the investigation of tearing mode interactions in cylindrical geometry. A set of equations describing the coupled evolution of the amplitude and phase of each mode in the plasma is obtained by combining electromagnetic and fluid flow information. Two interactions are investigated in detail as examples. The first example considered is the slowing down of a rotating magnetic island interacting with a resistive wall. Under certain conditions bifurcated steady state solutions are obtained, allowing the system to make sudden irreversible transitions from high rotation to low rotation states as the interaction strength is gradually increased, and vice versa. The second example considered is the interaction of a rotating tearing mode with a static external magnetic perturbation. In general, a rotating island is *stabilized* to some extent by the interaction, whereas a locked island is *destabilized*. In fact, a rotating island of sufficiently small saturated width can be completely stabilized. However, once the island width becomes too large, conventional mode locking occurs prior to complete stabilization. The interaction with a tearing-stable plasma initially gives rise to a modification of the bulk plasma rotation, with little magnetic reconnection induced at the rational surface. However, once a critical perturbation field strength is exceeded, there is a sudden change in the plasma rotation as a locked island is induced at the rational surface, with no rotating magnetic precursor. The implications of these results for typical ohmically heated tokamaks are evaluated. The comparatively slow mode rotation in large tokamaks renders such devices particularly sensitive to error-field induced locked modes, and the collapse of mode rotation due to wall interaction.

1. INTRODUCTION

Tearing modes occur in all conventional tokamaks and generally have a deleterious effect on plasma confinement properties. For instance, it is well known that the $m = 2, n = 1$ tearing mode is intimately associated with major disruptions [1]. Furthermore, it is a common occurrence for high performance plasmas to be degraded by the onset of strong tearing activity [2]. A better understanding of tearing mode stability, with a view to the possible control or suppression of such modes, is an important goal of international fusion research.

The basic theory of tearing modes is fairly well established. Tearing modes are thought to be helical magnetic perturbations, characterized by a poloidal mode number m (the number of periods in the poloidal direction) and a toroidal mode number n (the number of periods in the toroidal direction). Throughout the bulk of the plasma the perturbations obey the well known marginally stable ideal magnetohydrodynamic (MHD) equations [3]. However, these equations become singular on so-called 'rational' flux surfaces, where the magnetic winding number, or 'safety factor', q takes the rational value m/n . The ideal MHD singularities at

the rational surfaces are resolved by taking the plasma resistivity, viscosity and inertia into account [4]. The region of the plasma where ideal MHD breaks down is termed the 'inner region'. Likewise, the region of the plasma where ideal MHD holds is termed the 'outer region'. For non-ideal $m > 1$ modes, the breakdown of ideal MHD in the inner region permits the tearing and reconnection of equilibrium magnetic flux surfaces, to produce helical magnetic islands centred on the rational surfaces, whenever this process is energetically favourable [5]. The $m = 1$ mode generally requires special treatment [6] and is, therefore, not considered in this paper.

Non-interacting tearing modes in ohmically heated tokamaks usually propagate in the direction opposite to the equilibrium plasma current, with an associated rotation frequency of the order of the typical electron diamagnetic frequency [7]

$$f_{*e} \text{ (kHz)} \sim \frac{m}{2\pi} \frac{T_e \text{ (keV)}}{a^2 \text{ (m)} B_\phi \text{ (T)}}$$

where T_e is the electron temperature, a the minor radius and B_ϕ the toroidal field strength. Plasmas subjected to unbalanced neutral beam injection can develop bulk

toroidal rotation velocities that are orders of magnitude greater than typical diamagnetic velocities. In such plasmas, non-interacting tearing modes are observed to rotate in the direction of beam injection with velocities similar to that of the bulk plasma [8]. The marginally stable ideal MHD equations are unaffected by mode or plasma rotation, provided that the associated velocities remain subsonic and subAlfvénic [9], as is assumed to be the case throughout this paper.

The rotation frequency of a non-interacting tearing mode is termed the 'natural' mode frequency. In general, modes resonant on different rational surfaces have substantially different natural frequencies. This frequency mismatch can have a profound effect on the coupled evolution of the various modes in the plasma. Similarly, the frequency mismatch between a plasma mode and a stationary external structure, such as the vacuum vessel or a resonant error field, profoundly affects their mutual interaction.

The general non-linear tearing mode stability problem can be separated into two distinct parts. In the first part the perturbed marginally stable ideal MHD equations are solved in the outer region, subject to appropriate boundary conditions at the magnetic axis and the plasma boundary. External structures can usually be treated as modified edge boundary conditions. In general, the Fourier harmonics of the perturbed poloidal magnetic flux have gradient discontinuities at the various rational surfaces in the plasma, implying the existence of a helical current sheet flowing in the inner region in the vicinity of each surface. Such a current can interact with the local magnetic island in one of two ways. If it is in phase with the island it will modify the evolution of the island width. If it is in phase quadrature it will give rise to a $\mathbf{j} \times \mathbf{B}$ torque acting on the plasma in the vicinity of the island.

The second part of the non-linear stability problem deals with changes in the bulk plasma velocity associated with the deviations of the various island frequencies from their natural frequencies. At the simplest level, the various magnetic islands in the plasma can be treated as small obstacles entrained in a phenomenological (incompressible) viscous single fluid. The fluid is assumed to exert a viscous restoring torque if the island frequency deviates from its natural value. The single fluid equation of motion can be solved in the outer region subject to suitable boundary conditions at the magnetic axis and the plasma boundary. In this manner, the instantaneous viscous torque acting on each island region can be evaluated.

An equation of angular motion can be written for each island, in which the plasma inertia in the island

region is balanced against the sum of the local electromagnetic and viscous torques. Likewise, an evolution equation can be written for each island specifying how the width evolves under the influence of local in-phase sheet currents. These two sets of coupled equations completely specify the general non-linear tearing mode stability problem.

In Section 2 the various components of the scheme outlined above are worked out in *cylindrical* geometry. Poloidal flow damping, which is strictly speaking a toroidal effect, is included in the analysis in an ad hoc manner. In the remainder of the paper, two examples of tearing mode interactions are analysed in detail.

The first example considered (see Section 3) is the interaction of a rotating tearing mode with an external conductor (e.g. the vacuum vessel). This interaction has already been extensively studied in the literature [10–18]. The interaction of tearing modes with the vacuum vessel is thought to be responsible for the rapid slowing down of mode rotation that immediately precedes many types of tokamak disruptions [1, 16, 18].

The second example considered (see Section 5–7) is the interaction of a rotating plasma with an externally imposed *static* (i.e. non-rotating) helical magnetic perturbation. This interaction has also been extensively studied in the literature [18–25]. It is relevant to a series of experiments in which static helical magnetic perturbations (usually $m = 2$, $n = 1$) were applied to small tokamaks, via currents flowing in external windings, in order to affect, and possibly control, the intrinsic tearing mode activity [26–29]. Other related experiments have used external coils to induce bands of overlapping static tearing islands in the outer regions of the plasma (the so-called 'ergodic limiter'), in order to modify the edge conditions [30–32]. A low level of externally induced static helical magnetic perturbations (the so-called 'error field') is present in all tokamaks, owing to the inevitable slight misalignment of poloidal [33] and toroidal [34] field coils. Recent research [22] has suggested that the precursorless static tearing modes that significantly limit the disruption-free operating space, for low density ohmically heated discharges, in DIII-D [35] and JET [36], are due to interaction between the error field and the plasma.

The implications of some of the results derived in Sections 3–7 for typical ohmically heated tokamaks are discussed in Section 8. Finally, the paper is summarized in Section 9.

2. THE BASIC MODEL

2.1. Cylindrical tokamak equilibria

The conventional set of right handed cylindrical polar co-ordinates (r, θ, z) is employed. The (circular) equilibrium flux surfaces lie on surfaces of constant r . The system is assumed to be periodic in the z ('toroidal') direction, with periodicity length $2\pi R_0$, where R_0 is the simulated major radius. The safety factor $q = rB_z/R_0 B_\theta$, where B_z is the constant 'toroidal' field strength and $B_\theta(r)$ is the poloidal field strength. The equilibrium 'toroidal' current satisfies $\mu_0 j_z(r) = (rB_\theta)'/r$, where ' denotes $\partial/\partial r$. Finally, the standard large aspect ratio tokamak ordering, $(r/R_0) \ll 1$ and $(B_\theta/B_z) \ll 1$, is adopted.

2.2. Electromagnetic torques

The flux surface integrated poloidal and 'toroidal' electromagnetic torques acting on the plasma are given by

$$T_{\theta EM} = \int r \mathbf{j} \times \mathbf{B} \cdot \hat{\theta} dS \equiv \oint_0^{2\pi R_0} r \mathbf{j} \times \mathbf{B} \cdot \hat{\theta} r d\theta dz \quad (1a)$$

$$T_{z EM} = \int R_0 \mathbf{j} \times \mathbf{B} \cdot \hat{z} dS \quad (1b)$$

The marginally stable ideal MHD equations incorporate $\mathbf{j} \times \mathbf{B} = \nabla p$ [3]. It follows immediately from the form of Eqs (1a, b) and from the assumed periodicity of the system in the poloidal and 'toroidal' directions that $T_{\theta EM}$ and $T_{z EM}$ are zero in the region of the plasma governed by ideal MHD (i.e. the outer region). Thus, any net electromagnetic torques acting on the plasma must develop in the vicinity of the rational surfaces, where ideal MHD breaks down and large perturbed helical currents flow (i.e. in the inner region) [12].

Consider a general (m, n) magnetic perturbation

$$\delta \mathbf{B} = \delta B(r) \exp(i\xi) \quad (2)$$

where $\xi = m\theta - nz/R_0 - \int^t \omega(t') dt'$, and $\omega(t)$ is the instantaneous mode (angular) rotation frequency. (For the moment, it is assumed that there is only a single frequency ω in the problem, for the sake of simplicity. Later on (from Section 2.4 onwards), the analysis is generalized to allow for the many different frequencies ω_s associated with magnetic islands located at the various rational surfaces of radii r_s .) The perturbed current $\delta \mathbf{j}$ is also assumed to be of this form. Suppose that the large perturbed helical currents flowing in the vicinity of rational flux surfaces are 'sheet'-like (i.e. $|\delta j_r| \ll |\delta j_\theta|$,

$|\delta j_z|$ in the inner region). Equation (2), the Ampère-Maxwell equation, and current conservation ($\nabla \cdot \delta \mathbf{j} = 0$) imply that

$$i \left(\frac{m}{r} \delta B_z + \frac{n}{R_0} \delta B_\theta \right)_{r_k} = \mu_0 \delta j_r(r_k) \approx 0 \quad (3a)$$

$$i \left(\frac{n}{R_0} \delta j_z - \frac{m}{r} \delta j_\theta \right)_{r_k} = \frac{1}{r} \frac{\partial}{\partial r} [r \delta j_r(r_k)] \approx 0 \quad (3b)$$

Here, the r_k are the radii of the various rational surfaces (i.e. $q(r_k) = m/n$). The above equations yield $\delta \mathbf{B} \cdot \mathbf{B}_0 \approx 0$ (i.e. $\delta B_\parallel \approx 0$) and $\delta \mathbf{j} \propto \mathbf{B}_0$ (i.e. $\delta j_\perp \approx 0$) in the inner region, where \mathbf{B}_0 is the equilibrium field. More generally,

$$|\nabla_\parallel|_{r_k} \sim O \left(\frac{n}{R_0} \frac{s_k}{r_k} W_k \right) \quad (4a)$$

$$|\nabla_\perp|_{r_k} \sim O \left(\frac{1}{W_k} \right) \quad (4b)$$

in the vicinity of a rational surface r_k [19, 29], where W_k is the island width (i.e. the approximate width of that portion of the inner region centred on r_k) and $s_k \equiv (rq'/q)_{r_k}$ is the local magnetic shear. Thus, current conservation ($\nabla \cdot \delta \mathbf{j} \equiv \nabla_\parallel \delta j_\parallel + \nabla_\perp \cdot \delta \mathbf{j}_\perp = 0$) gives

$$\left| \frac{\delta j_\perp}{\delta j_\parallel} \right|_{r_k} \sim O \left(\epsilon \frac{W_k^2}{a^2} \right) \quad (5)$$

where $\epsilon = a/R_0 \ll 1$ is the inverse aspect ratio. For sufficiently small islands, Eq. (5) justifies the previous assumption that δj_r is negligible in the inner region.

Electromagnetic torques can also develop outside the plasma due, for instance, to eddy currents induced in conducting walls or helical currents flowing around external windings. If the system is cylindrically symmetric and if these external currents are localized in radius (i.e. any walls or external windings are thin), then the external currents are also 'sheet'-like and Eqs (3a, b) apply wherever an electromagnetic torque develops in the system (i.e. the r_k become the radii of any rational surfaces inside the plasma and the radii of any conducting walls or helical windings outside the plasma). The inner region is extended to include those regions where the external helical currents flow. Likewise, the outer region is extended to include those regions outside the plasma where no helical currents flow. Clearly, in a cylindrically symmetric system the external 'sheet' eddy currents induced by an (m, n) tearing mode have the same helical pitch as the equilibrium magnetic field at the rational surfaces inside the plasma. Similarly, this is the optimal pitch for external helical windings interacting with (m, n) modes.

It follows from the previous discussion that

$$T_{\theta EMk}(r) \approx \sum_k T_{\theta EMk} \delta(r - r_k) \quad (6a)$$

$$T_{z EMk}(r) \approx \sum_k T_{z EMk} \delta(r - r_k) \quad (6b)$$

where $T_{\theta EMk}$ and $T_{z EMk}$ are the components of the total electromagnetic torque which develops in that portion of the inner region centred on r_k (extent r_{k-} to r_{k+} , say). Equations (1a, b), (3a, b) and (6a, b) yield

$$T_{\theta EMk} = \int_{r_{k-}}^{r_{k+}} r \times \frac{1}{2} \int (\delta j_z \delta B_r^* + \delta j_z^* \delta B_r) dS dr \quad (7a)$$

$$T_{z EMk} = \int_{r_{k-}}^{r_{k+}} (-R_0) \times \frac{1}{2} \int (\delta j_\theta \delta B_r^* + \delta j_\theta^* \delta B_r) dS dr$$

$$= -\frac{n}{m} T_{\theta EMk} \quad (7b)$$

implying that the ratio of poloidal to ‘toroidal’ torques is $(-m/n)$ in all parts of the inner region.

2.3. The cylindrical tearing mode equation

In the large aspect ratio limit, $\epsilon \rightarrow 0$, the perturbed magnetic field can be written

$$\delta \mathbf{B} = \nabla \times (\Psi \hat{z}) \equiv \left(i \frac{m}{r} \Psi, -\frac{\partial \Psi}{\partial r}, 0 \right) \quad (8)$$

where $\Psi \equiv \psi(r) \exp(i\xi)$ is (proportional to) the perturbed poloidal magnetic flux. The cylindrical tearing mode equation, obtained by linearizing the perturbed ‘toroidal’ component of the marginally stable ideal MHD relation $\nabla \times (\mathbf{j} \times \mathbf{B}) = 0$, takes the form

$$\frac{1}{r} \frac{\partial}{\partial r} \left(r \frac{\partial \psi}{\partial r} \right) - \frac{m^2}{r^2} \psi + \frac{q_s \mu_0 j_z'}{B_\theta (q - q_s)} \psi = 0 \quad (9)$$

where $q_s = m/n$. Equation (9) is valid throughout the outer region, including the vacuum region ($j_z = 0$) outside the plasma. Suitable boundary conditions are that ψ is well behaved in the vicinity of the magnetic axis, and bounded as $r \rightarrow \infty$. Thus,

$$\psi(0) = \psi(\infty) = 0 \quad (10)$$

The ‘constant ψ ’ approximation, which is standard in the analysis of tearing modes [4], implies that the perturbed flux is approximately constant across each part of the inner region; i.e.

$$\psi(r_{k-}) = \psi(r_{k+}) = \psi_k \quad (11)$$

where ψ_k is the approximately constant value of ψ in that portion of the inner region centred on r_k .

Equation (9) can be solved in the outer region, subject to the constraints (10) and (11). In general, the first derivative of ψ is discontinuous at the various boundaries between the inner and outer regions. These discontinuities are associated with the ‘sheet-like’ currents flowing in the inner region. It is easily demonstrated that

$$\delta J_{zk} = \int_{r_{k-}}^{r_{k+}} \int \exp(-i\xi) \delta j_z dS dr$$

$$= -4\pi^2 R_0 \frac{1}{2\mu_0} \left[r \frac{\partial \psi}{\partial r} \right]_{r_{k-}}^{r_{k+}} \quad (12)$$

It follows from Eqs (7a, b), (8), (11) and (12) that

$$T_{\theta EMk} = 4\pi^2 R_0 \frac{m}{\mu_0} \frac{i}{4} \left\{ \left[r \frac{\partial \psi}{\partial r} \right]_{r_{k-}}^{r_{k+}} \psi_k^* \right. \\ \left. - \left[r \frac{\partial \psi^*}{\partial r} \right]_{r_{k-}}^{r_{k+}} \psi_k \right\} \quad (13)$$

Now, a trivial manipulation of Eq. (9) yields

$$\psi^* \frac{\partial}{\partial r} \left(r \frac{\partial \psi}{\partial r} \right) - \psi \frac{\partial}{\partial r} \left(r \frac{\partial \psi^*}{\partial r} \right)$$

$$\equiv \frac{\partial}{\partial r} \left(r \frac{\partial \psi}{\partial r} \psi^* - r \frac{\partial \psi^*}{\partial r} \psi \right) = 0 \quad (14)$$

Integration over the outer region, invoking the previously mentioned boundary conditions for ψ , gives

$$\sum_k \left\{ \left[r \frac{\partial \psi}{\partial r} \right]_{r_{k-}}^{r_{k+}} \psi_k^* - \left[r \frac{\partial \psi^*}{\partial r} \right]_{r_{k-}}^{r_{k+}} \psi_k \right\} = 0 \quad (15)$$

A comparison of Eqs (7a, b), (13) and (15) leads to

$$\sum_k T_{\theta EMk} = -\frac{m}{n} \sum_k T_{z EMk} = 0 \quad (16)$$

Thus, in accordance with Newton’s third law of motion, there is zero net electromagnetic torque acting on the system.

2.4. The Rutherford island evolution equation

If $\psi(r)$ is non-zero at a given rational surface within the plasma (radius r_s , say, where the r_s are the subset of the r_k that lie inside the plasma), then a chain of magnetic islands is formed. The maximum island width is given by

$$W_s = 4 \left(\frac{R_0 q_s}{B_z} \right)^{1/2} \left| \frac{\psi_s}{s_s} \right|^{1/2} \quad (17)$$

where ψ_s is the approximately constant value of ψ in that portion of the inner region centred on r_s . If the local magnetic shear s_s is positive, then the island O points are located at

$$\begin{aligned} & \left(m\theta - n \frac{z}{R_0} - \int' \omega_s(t') dt' \right)_{\text{O point}} \\ & = (2l - 1)\pi - \arg(\psi_s) \end{aligned} \quad (18)$$

and the X points at

$$\begin{aligned} & \left(m\theta - n \frac{z}{R_0} - \int' \omega_s(t') dt' \right)_{\text{X point}} \\ & = 2l\pi - \arg(\psi_s) \end{aligned} \quad (19)$$

and vice versa if the shear is negative. Here, $\omega_s(t)$ is the instantaneous rotation frequency of the chain of magnetic islands at r_s and l is a general integer.

Rutherford's well known non-linear island width evolution equation [5] can be written as

$$I_1 \tau_R(r_s) \frac{d}{dt} \left(\frac{W_s}{r_s} \right) = \Delta'_s r_s \quad (20)$$

where $I_1 = 0.8227$,

$$\tau_R(r_s) = \frac{\mu_0 r_s^2}{\eta_{\parallel}(r_s)} \quad (21)$$

and

$$\Delta'_s r_s = \left(\left\{ \left[r \frac{\partial \psi}{\partial r} \right]_{r_{s-}}^{r_{s+}} \psi_s^* + \left[r \frac{\partial \psi^*}{\partial r} \right]_{r_{s-}}^{r_{s+}} \psi_s \right\} / 2\psi_s \psi_s^* \right) \quad (22)$$

(Note that the value of I_1 quoted above is the exact value, rather than the approximate value quoted in Ref. [5].) The width of that portion of the inner region centred on r_s is approximately W_s [19], so $r_{s-} \approx r_s - W_s/2$ and $r_{s+} \approx r_s + W_s/2$.

In this paper, modifications to tearing mode stability due to plasma velocity shear [19, 29, 37, 38] are neglected. This is reasonable for subAlfvénic flows, provided that the velocity shear scale length does not become much smaller than the minor radius. This is likely to be the case in plasmas with an anomalous viscosity, where the viscous diffusion time-scale tends to be less than the magnetic reconnection time-scale (see Section 8).

2.5. Viscous torques

The various magnetic islands in the plasma are effectively treated as solid body obstacles entrained in a phenomenological (incompressible) viscous single fluid.

The interaction of a non-linear magnetic island with the external plasma is similar to that of a solid body because there is no net plasma flow across the island separatrix (i.e. the island does not 'slip' through the

plasma). This is demonstrated for a single fluid plasma in Ref. [19], where the cross-flux surface flows around a magnetic island not propagating at its natural frequency are found to be eddy-like (i.e. with no directed component in the island frame of reference). This result is valid as long as the island width is significantly larger than the linear layer width (i.e. as long as the concept of a magnetic island is meaningful) (see Section 7.1).

For a multifluid plasma, the 'no-slip' constraint implies that the *relative* propagation velocity of the magnetic island with respect to the various plasma fluids is unaffected by the locally applied electro-magnetic torque. This is reasonable, since in standard tearing mode theory the relative propagation velocity of the perturbed magnetic field is determined by the *parallel* (to the local equilibrium magnetic field) Ohm's law [39], whereas the electromagnetic torque acts in the *perpendicular* direction. The 'no-slip' constraint has been verified experimentally [40].

The single fluid treatment of the plasma is justified as long as the analysis is only concerned with *changes* in plasma velocity brought about by *deviations* of the various island frequencies from their natural values. Under normal tokamak operating conditions, the velocities of the various fluids that comprise the plasma (e.g. the fuelling ion fluid, the electron fluid) are strongly coupled, owing to the requirement that the net plasma current remains approximately constant. To a first approximation, a velocity change in one fluid is likely to be matched by equal velocity changes in all of the other fluids. This view is supported by experiments performed on the COMPASS-C tokamak, which suggest that changes in the phenomenological single fluid toroidal velocity, inferred from island frequency shifts, are matched by changes in the impurity ion toroidal velocity, measured by spectroscopic means [29].

If there is no net plasma flow across the various island separatrices, then $\Delta\Omega_\theta$ and $\Delta\Omega_z$ are approximately constant across each portion of the inner region lying inside the plasma (i.e. from r_{s-} to r_{s+} , for all r_s). Here, $[0, \Delta\Omega_\theta(r), \Delta\Omega_z(r)]$ is the flux surface averaged change in the phenomenological single fluid (angular) velocity due to deviations of the island frequencies from their natural values. It follows from continuity requirements that

$$\Delta\Omega_\theta(r_{s-}) = \Delta\Omega_\theta(r_{s+}) = \Delta\Omega_{\theta_s} \quad (23a)$$

$$\Delta\Omega_z(r_{s-}) = \Delta\Omega_z(r_{s+}) = \Delta\Omega_{z_s} \quad (23b)$$

where $\Delta\Omega_{\theta_s}$ and $\Delta\Omega_{z_s}$ are approximately constant values of $\Delta\Omega_\theta$ and $\Delta\Omega_z$, respectively, in that portion of the

inner region centred on r_s . It is easily demonstrated that for a 'non-slipping' island

$$m\Delta\Omega_{\theta s} - n\Delta\Omega_{zs} = \Delta\omega_s \equiv \omega_s - \omega_{0s} \quad (24)$$

where $\Delta\omega_s$ represents a deviation of the island (angular) frequency ω_s from its natural value ω_{0s} .

It is assumed that changes in the single fluid (angular) velocity associated with deviations of the various island frequencies from their natural values are opposed by the perpendicular viscosity [41] and by poloidal flow damping [42]. Thus, the following flux surface averaged equation of (angular) motion of the phenomenological single fluid is adopted:

$$\rho \frac{\partial \Delta\Omega_{\theta}}{\partial t} = \frac{1}{r^3} \frac{\partial}{\partial r} \left((\mu_{\perp} r^3) \frac{\partial \Delta\Omega_{\theta}}{\partial r} \right) - \frac{\rho}{\tau_D} \Delta\Omega_{\theta} \quad (25a)$$

$$\rho \frac{\partial \Delta\Omega_z}{\partial t} = \frac{1}{r} \frac{\partial}{\partial r} \left((\mu_{\perp} r) \frac{\partial \Delta\Omega_z}{\partial r} \right) \quad (25b)$$

Here, $\rho(r)$ is the plasma density, $\mu_{\perp}(r)$ is the (anomalous) coefficient of perpendicular viscosity and $\tau_D(r)$ is the poloidal flow damping time-scale. The perpendicular viscosity operator follows from Braginskii [41] (for incompressible flow, with $\eta_1 = \eta_2 = \mu_{\perp}$); however, the poloidal flow damping operator is purely ad hoc. Equations (25a, b) are valid throughout that portion of the outer region that lies inside the plasma.

The boundary conditions

$$\Delta\Omega'_{\theta}(0) = \Delta\Omega'_z(0) = 0 \quad (26)$$

ensure that $\Delta\Omega_{\theta}$ and $\Delta\Omega_z$ are well behaved in the vicinity of the magnetic axis.

It is assumed that edge interactions (e.g. collisions with the limiter [43], or charge exchange with neutrals emitted isotropically from the wall [44]) are only significant in a thin boundary layer (thickness, δ_X , say) close to the limiter ($r = a$). It is further assumed that the average momentum exchange time between the plasma in the boundary layer and the wall/limiter is τ_X . It follows that the components of the total interaction torque which develops in the boundary layer take the form

$$T_{\theta\text{BL}} = -4\pi^2 R_0 \frac{\delta_X}{\tau_X} [(\rho r^3) \Delta\Omega_{\theta}]_a \quad (27a)$$

$$T_{z\text{BL}} = -4\pi^2 R_0 \frac{\delta_X}{\tau_X} [(\rho r R_0^2) \Delta\Omega_z]_a \quad (27b)$$

If the fluid inertia in the boundary layer is neglected, then the appropriate edge boundary conditions to Eqs (25a, b) are

$$\kappa_X \left[r \frac{\partial \Delta\Omega_{\theta}}{\partial r} \right]_a + (\Delta\Omega_{\theta})_a = 0 \quad (28a)$$

$$\kappa_X \left[r \frac{\partial \Delta\Omega_z}{\partial r} \right]_a + (\Delta\Omega_z)_a = 0 \quad (28b)$$

where

$$\kappa_X = \frac{\tau_X \mu_{\perp}(a)}{\delta_X a \rho(a)} \quad (29)$$

is (approximately) the ratio of the momentum diffusion velocity from the bulk fluid into the boundary layer to the momentum transmission velocity from the boundary layer to the wall/limiter. A simple model of the boundary layer is described in Appendix A.

Equations (25a, b) can be solved in that portion of the outer region lying inside the plasma, subject to the constraints (23a, b), (26) and (28a, b). In general, the first derivatives of $\Delta\Omega_{\theta}$ and $\Delta\Omega_z$ are discontinuous at the various boundaries between the inner and outer regions. These discontinuities are associated with the viscous torques acting on the inner region. It is easily demonstrated that

$$T_{\theta\text{VS}} = 4\pi^2 R_0 \left[(\mu_{\perp} r^3) \frac{\partial \Delta\Omega_{\theta}}{\partial r} \right]_{r_s^-}^{r_s^+} \quad (30a)$$

$$T_{z\text{VS}} = 4\pi^2 R_0 \left[(\mu_{\perp} r R_0^2) \frac{\partial \Delta\Omega_z}{\partial r} \right]_{r_s^-}^{r_s^+} \quad (30b)$$

where $T_{\theta\text{VS}}$ and $T_{z\text{VS}}$ are the components of the total viscous torque acting on that portion of the inner region in the vicinity of a rational surface r_s .

2.6. The island equation of angular motion

The equations of angular motion of an island in the vicinity of a rational surface r_s are obtained by balancing inertia against the sum of the local electromagnetic and viscous torques. Thus,

$$4\pi^2 R_0 \int_{r_s^-}^{r_s^+} (\rho r^3) dr \left(\frac{\partial \Delta\Omega_{\theta s}}{\partial t} \right) = T_{\theta\text{VS}} + T_{\theta\text{EMs}} \quad (31a)$$

$$4\pi^2 R_0 \int_{r_s^-}^{r_s^+} (\rho r R_0^2) dr \left(\frac{\partial \Delta\Omega_{zs}}{\partial t} \right) = T_{z\text{VS}} - \frac{n}{m} T_{\theta\text{EMs}} \quad (31b)$$

where use has been made of Eqs (7a, b). The poloidal flow damping torque is neglected in the inner region, since it is generally much smaller than the highly localized electromagnetic and viscous torques.

2.7. The global equation of angular motion

The global equation of (angular) motion of the plasma is obtained by integrating Eqs (25a, b) across that por-

tion of the outer region lying inside the plasma, and adding the results to the sum of Eqs (31a, b) over all rational surfaces. Thus,

$$4\pi^2 R_0 \int_0^a (\rho r^3) \left(\frac{\partial \Delta \Omega_\theta}{\partial t} + \frac{\Delta \Omega_\theta}{\tau_D} \right) dr$$

$$= - \sum_{k'} T_{\theta EM k'} - (-T_{\theta BL}) \quad (32a)$$

$$4\pi^2 R_0 \int_0^a (\rho r R_0^2) \frac{\partial \Delta \Omega_z}{\partial t} dr$$

$$= - \sum_{k'} T_{z EM k'} - (-T_{z BL}) \quad (32b)$$

where use has been made of Eq. (16). Here, the $r_{k'}$ are the subset of the r_k that lie outside the plasma, so $\sum_{k'} T_{\theta EM k'}$ and $\sum_{k'} T_{z EM k'}$ are the components of the total electromagnetic reaction torque acting on external structures (e.g. the vacuum vessel), whilst $(-T_{\theta BL})$ and $(-T_{z BL})$ are the components of the total reaction torque acting on the limiter or wall, owing to interaction with the edge boundary layer. Equations (32a, b) specify how the total inertia of any change in the single fluid flow set up by deviations of the various island frequencies from their natural values evolves under the influence of electromagnetic interactions with external structures (e.g. the vacuum vessel), interaction with the wall or limiter, and (simulated) poloidal flow damping. Clearly, in a steady state (i.e. $\partial/\partial t = 0$) the sum of all the 'toroidal' reaction torques acting externally to the plasma is zero. The same is not true of the poloidal reaction torques because the total poloidal angular momentum is not a conserved quantity in a (simulated) toroidal system.

2.8. Discussion of the basic model

The electromagnetic component of the model is fairly conventional. It is valid for low beta, circular cross-section, large aspect ratio tokamaks with 'thin' islands (i.e. $W/a \ll 1$). Asymptotic matching between the inner and outer regions is achieved using the 'constant ψ ' approximation. This rather crude level of matching gives rise to gradient discontinuities in the perturbed magnetic flux ψ at the boundaries between the inner and outer regions. In reality, the jumps in ψ' across the various parts of the inner region take place in a continuous manner. An improved electromagnetic asymptotic matching procedure is described in Ref. [45].

Although it utilizes Rutherford island theory, the model otherwise effectively treats magnetic islands

in the plasma as *annular* regions of width W_s , centred on the rational surfaces at r_s . It is assumed that the widths of the various parts of the inner region centred on the rational surfaces in the plasma are given by the corresponding island widths. A more sophisticated treatment is described in Ref. [19].

The fluid component of the model is novel, but is completely phenomenological in nature. The basic premise is that deviations of the various island frequencies from their natural values are opposed by the plasma perpendicular viscosity. This has been confirmed by experiments performed on the COMPASS-C tokamak [29]. The model does not attempt to predict the natural rotation frequencies of unperturbed modes. In fact, these natural frequencies must be regarded as inputs to the model.

In the fluid model, asymptotic matching between the inner and outer regions is achieved by assuming solid body rotation in the inner region. This fairly basic level of matching gives rise to velocity gradient discontinuities on the boundaries between the inner and outer regions. An improved fluid asymptotic matching procedure is described in Ref. [19].

Although the model is derived in *cylindrical* geometry, it is intended for use in the interpretation of data obtained from (low beta, large aspect ratio) *toroidal* devices. Poloidal flow damping, which turns out to be the most important toroidal effect, is simulated in an ad hoc manner. In toroidal geometry, any (incompressible) poloidal flow must be accompanied by toroidal 'return flows', since pure poloidal flow is not divergence free. This effect is not taken into account in the model. Toroidal coupling of the different poloidal harmonics of the outer ideal MHD solution is, likewise, not taken into account in the model.

In summary, the model outlined in the previous subsections is the simplest possible treatment of the general coupled tearing mode problem in cylindrical geometry which incorporates various physics features that are deemed to play an essential role in the problem. These essential features are as follows:

(a) Electromagnetic coupling of the various magnetic islands in the plasma, and any external structures (e.g. the vacuum vessel), via the marginally stable perturbed ideal MHD equations; island growth/decay governed by Rutherford theory.

(b) Substantially different natural frequencies of modes resonant on different rational surfaces in the plasma; a substantial frequency mismatch between plasma modes and static external structures.

(c) No ‘slipping’ of non-linear magnetic islands through the plasma; a viscous restoring torque acting on an island whose frequency deviates from its natural value.

(d) Viscous coupling across the plasma cross-section via bulk (anomalous) perpendicular plasma viscosity; momentum exchange between the edge of the plasma and the wall/limiter.

(e) Poloidal flow damping due to variations of the toroidal field strength around flux surfaces.

Note that Rutherford theory and the ‘no-slip’ constraint are only valid for *non-linear* magnetic islands, in which the island width is much larger than the linear layer width. In some situations, islands are prevented from entering the non-linear regime (i.e. the island width remains less than, or of the order of, the linear layer width), and a slightly different approach is required (see Section 7).

3. INTERACTION OF A ROTATING MAGNETIC ISLAND WITH A CONDUCTING WALL

3.1. Introduction

Consider the interaction of a general (m, n) tearing mode, resonant inside the plasma on a *single* flux surface of radius r_s , with a *single* cylindrically symmetric conducting wall of radius r_w ($r_w > a$), thickness δ_w ($\delta_w/r_w \ll 1$) and conductivity tensor **diag**(0, $\sigma_{w\theta\theta}$, σ_{wzz}). Anisotropic conductivity arises experimentally because many tokamaks possess vacuum vessels that are convoluted (i.e. bellows-like) in the toroidal direction, effectively decreasing the toroidal conductivity with respect to the poloidal conductivity.

Helical eddy currents induced in the wall by rotation of the tearing mode (angular frequency ω , say) give rise to a ‘jump’ in the derivative of the perturbed poloidal magnetic flux $\psi(r)$ across the wall. Thus,

$$\left[r \frac{\partial \psi}{\partial r} \right]_{r_w^-}^{r_w^+} = 2m\tau_w(-i\omega)\psi_w \quad (33)$$

[12, 15, 16, 46, 47], where ψ_w is the approximately constant value of ψ inside the wall, $r_{w\pm} = r_w \pm \delta_w/2$, and

$$\begin{aligned} \tau_w &= \frac{\mu_0}{2m} \left[\frac{1}{\sigma_{wzz}} + \left(\frac{r_w}{R_0 q_s} \right)^2 \frac{1}{\sigma_{w\theta\theta}} \right]^{-1} \delta_w r_w \\ &\approx \frac{\mu_0 \sigma_{wzz} \delta_w r_w}{2m} \end{aligned} \quad (34)$$

Formula (33) is valid, provided

$$\frac{\delta_w}{r_w} \ll m\omega\tau_w \ll \frac{r_w}{\delta_w} \quad (35)$$

Note that with the conventional tokamak ordering ($q_s \sim O(1)$, $r_w/R_0 \ll 1$) the interaction is governed almost entirely by the ‘toroidal’ wall conductivity σ_{wzz} .

It is assumed that the mode growth time-scale is much greater than the wall time constant τ_w , so that the ‘wall modes’ discussed in Refs [20] and [46] are excluded from consideration. This is reasonable, provided that the plasma is stable to free boundary ideal external kink modes.

3.2. The electromagnetic solution in the outer region

In the outer region, the perturbed poloidal flux $\psi(r)$ satisfies the cylindrical tearing mode equation (9), subject to the physical boundary conditions (10), with the continuity constraint (11) imposed at the rational surface and the constraint (33) imposed at the wall. Without loss of generality, $\psi(r)$ can be split into two parts. The first part, $\psi_{\text{mode}}(r)$, satisfies Eq. (9), the two physical boundary conditions and the continuity constraint, but has no gradient discontinuities at the wall. The second part, $\psi_{\text{wall}}(r)$, also satisfies Eq. (9), the physical boundary conditions and the continuity constraint, but is zero in the island region and is subject to the constraint (33) at the wall. In general, ψ_{wall} is zero for $r < r_{s+}$. The function $\psi_{\text{mode}}(r)$ is the standard free boundary cylindrical tearing mode basis function, representing a magnetic island at the rational surface. The function $\psi_{\text{wall}}(r)$ represents the *ideal* MHD response of the plasma to the helical currents induced in the wall.

If the equilibrium plasma current is mostly concentrated inside the mode rational surface, so that $j_z(r > r_{s+}) \approx 0$ (this is usually a fairly good approximation for the (2, 1), (3, 1) modes, etc.), then it is easily demonstrated that

$$\psi_{\text{mode}}(r) \approx \Psi \left(\frac{r}{r_{s+}} \right)^{-m} \quad (36a)$$

for $r_{s+} < r$

$$\begin{aligned} \psi_{\text{wall}}(r) &\approx \Psi \left[\left(\frac{r}{r_{s+}} \right)^m - \left(\frac{r}{r_{s+}} \right)^{-m} \right] \\ &\times \frac{i(\omega\tau_w)(r_{s+}/r_w)^{2m}}{1 - i(\omega\tau_w)[1 - (r_{s+}/r_w)^{2m}]} \end{aligned} \quad (36b)$$

for $r_{s+} < r < r_w$ and

$$\psi_{\text{wall}}(r) \approx \Psi \left(\frac{r}{r_{s+}} \right)^{-m} \frac{i(\omega\tau_w)[1 - (r_{s+}/r_w)^{2m}]}{1 - i(\omega\tau_w)[1 - (r_{s+}/r_w)^{2m}]} \quad (36c)$$

for $r_w < r$, where the finite width of the wall has been neglected. Here, the 'reconnected magnetic flux' Ψ is the approximately constant value of ψ in the island region. The reconnected flux is related to the island width W via

$$W = 4 \left(\frac{R_0 q_s}{B_z} \right)^{1/2} \left| \frac{\Psi}{S_s} \right|^{1/2} \quad (37)$$

The 'toroidal' component of the 'sheet' current flowing in the island region owing to the presence of the conducting wall (i.e. the helical current at r_s due to ψ_{wall}) is given by

$$\begin{aligned} \delta J_{z,s,\text{wall}} &\approx 4\pi^2 R_0 \frac{m}{\mu_0} \\ &\times \frac{(\omega\tau_w)^2 (r_{s+}/r_w)^{2m} [1 - (r_{s+}/r_w)^{2m}] - i(\omega\tau_w)(r_{s+}/r_w)^{2m}}{1 + (\omega\tau_w)^2 [1 - (r_{s+}/r_w)^{2m}]^2} \Psi \end{aligned} \quad (38)$$

where use has been made of Eq. (12) and the approximation (36a-c). As will become apparent, the part of $\delta J_{z,s,\text{wall}}$ that is in phase with the island (i.e. in phase with Ψ , see Eqs (18) and (19)) modifies the island stability, whereas the part that is in phase quadrature gives rise to a $\mathbf{j} \times \mathbf{B}$ torque acting on the island.

The tearing stability index of the mode can be written as

$$\Delta'_s = \Delta'_{\text{mode}} + \Delta'_{\text{wall}} \quad (39)$$

where

$$\Delta'_{\text{mode}} r_s = \left[r \frac{\partial |\psi_{\text{mode}}|}{\partial r} \right]_{r_{s-}}^{r_{s+}} / |\Psi| \quad (40)$$

is the standard stability index for a free boundary tearing mode, and

$$\Delta'_{\text{wall}} r_s \approx -2m \frac{(\omega\tau_w)^2 (r_{s+}/r_w)^{2m} [1 - (r_{s+}/r_w)^{2m}]}{1 + (\omega\tau_w)^2 [1 - (r_{s+}/r_w)^{2m}]^2} \quad (41)$$

parameterizes the *stabilizing* effect of the conducting wall on the rotating mode. Here, use has been made of Eq. (22) and the approximation (36a-c).

The poloidal electromagnetic torque acting on the island is given by

$$T_{\theta,EMs} \approx -4\pi^2 R_0 \frac{m^2}{\mu_0} \frac{(\omega\tau_w)(r_{s+}/r_w)^{2m}}{1 + (\omega\tau_w)^2 [1 - (r_{s+}/r_w)^{2m}]^2} |\Psi|^2 \quad (42)$$

where use has been made of Eq. (13) and the approximation (36a-c). Clearly, the electromagnetic torque always acts so as to *slow down* the island rotation.

In principle, Δ'_{mode} , Δ'_{wall} and $T_{\theta,EMs}/|\Psi|^2$ are all functions of the island width W , through their dependence on $r_{s\pm} = r_s \pm W/2$. However, according to Eqs (41) and (42), the variations of Δ'_{wall} and $T_{\theta,EMs}/|\Psi|^2$ with island width are negligible in the thin island limit $W/a \ll 1$. On the other hand, the variation of Δ'_{mode} with island width cannot be neglected, since it is responsible for the non-linear saturation of the tearing mode [45]. This effect can be simulated by writing

$$\Delta'_{\text{mode}}(W) \approx \Delta'_{\text{mode}}(0) \left(1 - \frac{W}{W_0} \right) \quad (43)$$

where W_0 is the zero frequency (i.e. free boundary) saturated island width. Experiments performed on the COMPASS-C tokamak have verified that Eq. (43) is a good description of the island saturation [29].

3.3. The steady state fluid solution in the outer region

In the outer region, the fluid velocity shift satisfies Eqs (25a, b), subject to the boundary conditions (26) and (28a, b), and the continuity constraints (23a, b). In the strong poloidal flow damping limit, the most general *steady state* (i.e. $\partial/\partial t = 0$) solution is

$$\Delta\Omega_{\theta}(r) \approx \Delta\Omega_{\theta,s} \exp\left(-\frac{(r_{s-} - r)}{\delta_{D-}}\right) \quad (44a)$$

for $0 < r < r_{s-}$

$$\Delta\Omega_{\theta}(r) \approx \Delta\Omega_{\theta,s} \exp\left(-\frac{(r - r_{s+})}{\delta_{D+}}\right) \quad (44b)$$

for $r_{s+} < r < a$

$$\Delta\Omega_z(r) = \Delta\Omega_{z,s} \quad (44c)$$

for $0 < r < r_{s-}$ and

$$\Delta\Omega_z(r) = \Delta\Omega_{z,s} \frac{\int_r^a [\mu_{\perp}(a)/\mu_{\perp}(r')] dr'/r' + \kappa_X}{\int_{r_{s+}}^a [\mu_{\perp}(a)/\mu_{\perp}(r')] dr'/r' + \kappa_X} \quad (44d)$$

for $r_{s+} < r < a$, where

$$\frac{\delta_{D\pm}}{a} = \left(\frac{\mu_{\perp}}{a^2 \rho} \tau_D \right)_{r_{s\pm}}^{1/2} \quad (45)$$

Here, $\Delta\Omega_{\theta,s}$ and $\Delta\Omega_{z,s}$ are the approximately constant fluid (angular) velocity shifts in the island region. The 'toroidal' velocity shift profile is solid-body-like inside the rational surface, but sheared outside. The shear becomes increasingly weak as the drag on the plasma due to interaction with the wall/limiter decreases (i.e. as κ_X increases). In the limit where this drag is zero

(i.e. $\kappa_X \rightarrow \infty$) the whole plasma rotates 'toroidally' as a solid body. The poloidal velocity shift profile is localized around the rational surface, owing to the action of strong poloidal flow damping. Note that the above expression for $\Delta\Omega_\theta(r)$ is only valid in the limit where the localization length scales $\delta_{D\pm}$ are much less than the minor radius.

The components of the steady state viscous restoring torque acting on the island are given by

$$T_{\theta \text{ vs } s} \approx -4\pi^2 R_0 \Delta\Omega_{\theta s} \left(\frac{\mu_\perp(r_{s-})r_{s-}^3}{\delta_{D-}} + \frac{\mu_\perp(r_{s+})r_{s+}^3}{\delta_{D+}} \right) \quad (46a)$$

$$T_{z \text{ vs } s} = -4\pi^2 R_0 \Delta\Omega_{z s} \mu_\perp(a) R_0^2 \left(\int_{r_{s+}}^a \frac{\mu_\perp(r')}{\mu_\perp(r')} \frac{dr'}{r'} + \kappa_X \right) \quad (46b)$$

where use has been made of Eqs (30a, b) and (44a-d). It is easily demonstrated that in the thin island limit ($W/a \ll 1$) the variations of $T_{\theta \text{ vs } s}$ and $T_{z \text{ vs } s}$ with island width are negligible.

3.4. Steady state island solution

3.4.1. The steady state island width

The Rutherford island equation (20) reduces to

$$\frac{W}{W_0} = \frac{1 + 3\beta\hat{\omega}^2}{1 + 3\hat{\omega}^2} \quad (47)$$

for a steady state in the thin island limit, where use has been made of Eqs (39), (41) and (43). Here,

$$\hat{\omega} = \frac{\omega\tau_w}{\sqrt{3}} \left[1 - \left(\frac{r_s}{r_w} \right)^{2m} \right] \quad (48a)$$

$$\beta = 1 + \frac{\Delta'_{\text{wall}}(\omega \rightarrow \infty)}{\Delta'_{\text{mode}}(W \rightarrow 0)} < 1 \quad (48b)$$

It follows from Eq. (47) that the high frequency (i.e. ideal wall) saturated island width, W_∞ , is given by

$$W_\infty = \beta W_0 \quad (49)$$

for $\beta > 0$. For $\beta < 0$, the mode is *stable* in the high frequency limit.

3.4.2. The steady state fluid velocity shifts

The ratio of the steady state velocity shifts in the island region are evaluated by eliminating $T_{\theta \text{ EM } s}$ from the island equations of motion (31a, b) and then making use of Eqs (46a, b). Thus,

$$\frac{\Delta\Omega_{\theta s}}{\Delta\Omega_{z s}} = -\frac{1}{2} \frac{\delta_D}{r_s} \frac{q_s}{\epsilon_s^2} \left/ \left(\int_{r_s}^a \frac{\mu_\perp(r')}{\mu_\perp(r')} \frac{dr'}{r'} + \frac{\mu_\perp(r_s)}{\mu_\perp(a)} \kappa_X \right) \right. \quad (50)$$

in the thin island limit. Here, $\epsilon_s = r_s/R_0$. In a plasma subject to weak poloidal flow damping the ratio of the poloidal to the 'toroidal' velocity shifts is large, up to a maximum value of $O(q_s/\epsilon_s^2)$ for a plasma where poloidal flow damping is absent. However, for a plasma subject to strong flow damping (i.e. $\delta_D \ll a$) the ratio is much reduced and may even become less than unity. The ratio is reduced even further if the drag on the plasma due to interaction with the wall/limiter becomes weak (i.e. $\kappa_X \rightarrow \infty$), so that the plasma can rotate freely as a solid body in the 'toroidal' direction.

3.4.3. The steady state island frequency

The relation between the steady state island frequency ω and the natural frequency ω_0 is obtained from the island equations of motion (31a, b) and the 'no-slip' constraint (24), using Eqs (37), (42), (46a, b) and (50). Thus,

$$\hat{\omega}_0 = \hat{\omega} \left(1 + 8\hat{W}_0^4 \frac{(1 + 3\beta\hat{\omega}^2)^4}{(1 + 3\hat{\omega}^2)^5} \right) + \Gamma \quad (51)$$

where

$$\Gamma = \tau_V \frac{\partial \hat{\omega}}{\partial t} \frac{W}{r_s} \left[\left(\int_{r_s}^a \frac{\mu_\perp(r')}{\mu_\perp(r')} \frac{dr'}{r'} + \frac{\mu_\perp(r_s)}{\mu_\perp(a)} \kappa_X \right)^2 + \left(\frac{1}{2} \frac{\delta_D}{r_s} \right)^2 \left(\frac{q_s}{\epsilon_s} \right)^2 \right] \left/ \left[\left(\int_{r_s}^a \frac{\mu_\perp(r')}{\mu_\perp(r')} \frac{dr'}{r'} + \frac{\mu_\perp(r_s)}{\mu_\perp(a)} \kappa_X \right) + \left(\frac{1}{2} \frac{\delta_D}{r_s} \right) \left(\frac{q_s}{\epsilon_s} \right)^2 \right] \right. \quad (52a)$$

$$\hat{\omega}_0 = \frac{\omega_0 \tau_w}{\sqrt{3}} \left[1 + \left(\frac{r_s}{r_w} \right)^{2m} \right] \quad (52b)$$

$$\hat{W}_0 = \frac{W_0}{W_{\text{wall}_1}} \quad (52c)$$

$$\frac{W_{\text{wall}_1}}{r_s} = \left[\frac{2^{11}}{m} \mathfrak{F}_{\text{steady}} \left(\frac{r_w}{r_s} \right)^{2m} \frac{\tau_H^2}{\tau_w \tau_V} \right]^{1/4} \quad (52d)$$

$$\mathfrak{F}_{\text{steady}} = \left(\frac{q_s}{\epsilon_s} \right)^2 \left/ \left[\frac{1}{2} \frac{\delta_D}{r_s} \left(\frac{q_s}{\epsilon_s} \right)^2 + \int_{r_s}^a \frac{\mu_\perp(r')}{\mu_\perp(r')} \frac{dr'}{r'} + \frac{\mu_\perp(r_s)}{\mu_\perp(a)} \kappa_X \right] \right. \quad (52e)$$

$$\tau_H = \frac{R_0 \sqrt{\mu_0 \rho(r_s)}}{B_z n_s} \quad (52f)$$

$$\tau_V = \frac{r_s^2 \rho(r_s)}{\mu_\perp(r_s)} \quad (52g)$$

Here, τ_H is the local hydromagnetic time-scale at the rational surface and τ_V is a typical viscous diffusion

time-scale in the vicinity of the rational surface. Note that

$$\delta_D/r_s = \sqrt{\tau_D(r_s)/\tau_V}$$

(see Eq. (45)), so the above solution is only valid in the limit where the typical poloidal flow damping time-scale is much less than the viscous diffusion time-scale. The function $\mathfrak{F}_{\text{steady}}$ parametrizes the effects of poloidal flow damping and wall/limiter interaction for steady state velocity shift profiles.

The inertia operator Γ is retained in Eq. (51) in order to analyse the stability of solutions. In fact, the solutions are stable provided that

$$\frac{\partial \hat{\omega}}{\partial \Gamma} (\Gamma = 0) < 0 \quad (53)$$

i.e. if the normalized frequency $\hat{\omega}$ is just below the steady state value then $\partial \hat{\omega} / \partial \tau > 0$, and vice versa. Application of Eq. (53) gives the stability criterion

$$6\hat{\omega}^3 \frac{[4\beta - 5 - 3\beta\hat{\omega}^2]}{[1 + 27(\beta - 1)\hat{\omega}^2 - 9\beta\hat{\omega}^4]} - \hat{\omega}_0 > 0 \quad (54)$$

3.4.4. Description of the steady state solutions

Figures 1(a-c) show steady state solutions of Eq. (51) plotted as contours of constant \hat{W}_0 (normalized island width) in the $\hat{\omega}$ (normalized mode frequency) versus $\hat{\omega}_0$ (normalized natural frequency) plane, for three values of β ; $\beta = 1$, corresponding to ineffective wall stabilization; $\beta = 0$, corresponding to a wall stabilization

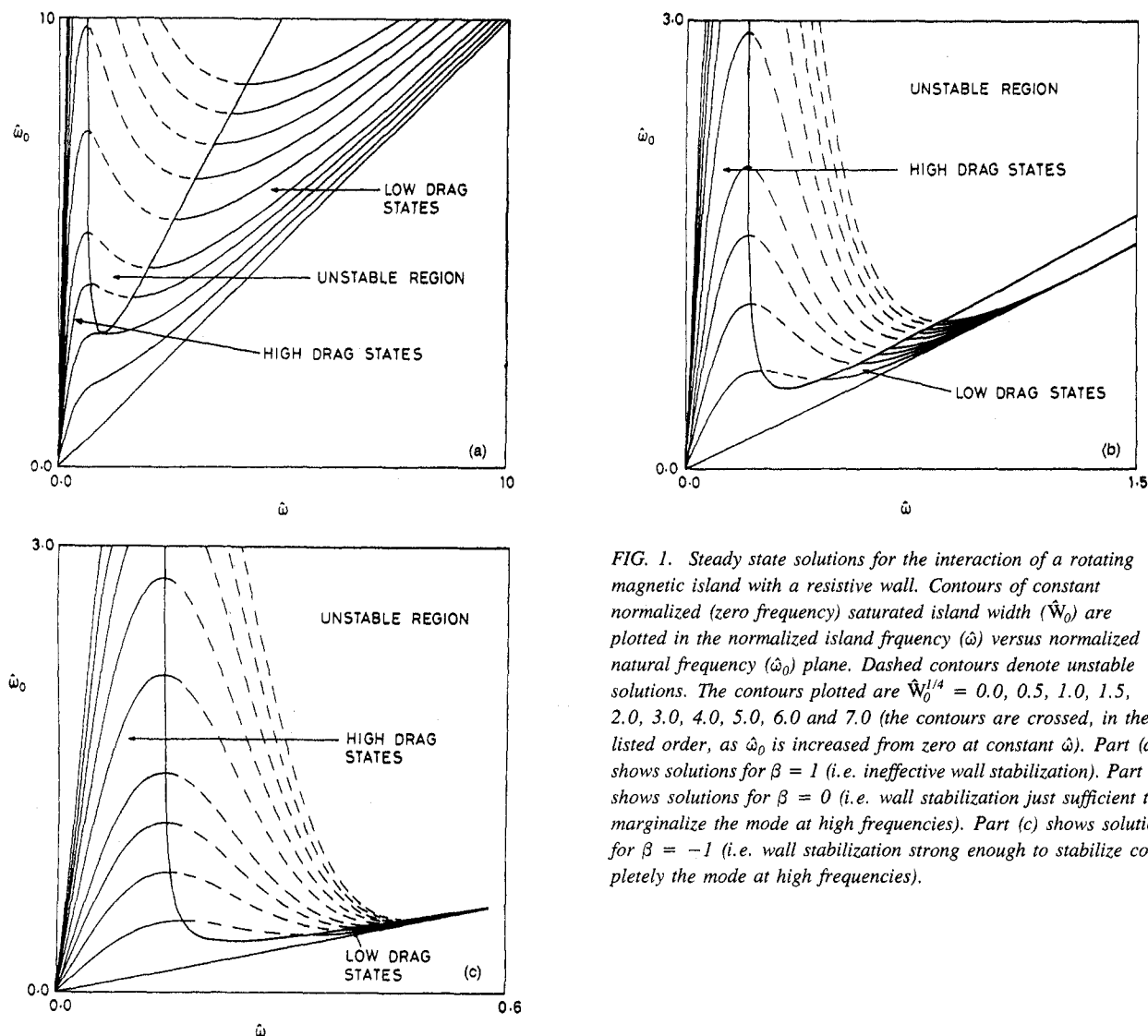


FIG. 1. Steady state solutions for the interaction of a rotating magnetic island with a resistive wall. Contours of constant normalized (zero frequency) saturated island width (\hat{W}_0) are plotted in the normalized island frequency ($\hat{\omega}$) versus normalized natural frequency ($\hat{\omega}_0$) plane. Dashed contours denote unstable solutions. The contours plotted are $\hat{W}_0^{1/4} = 0.0, 0.5, 1.0, 1.5, 2.0, 3.0, 4.0, 5.0, 6.0$ and 7.0 (the contours are crossed, in the listed order, as $\hat{\omega}_0$ is increased from zero at constant $\hat{\omega}$). Part (a) shows solutions for $\beta = 1$ (i.e. ineffective wall stabilization). Part (b) shows solutions for $\beta = 0$ (i.e. wall stabilization just sufficient to marginalize the mode at high frequencies). Part (c) shows solutions for $\beta = -1$ (i.e. wall stabilization strong enough to stabilize completely the mode at high frequencies).

TABLE I. CRITICAL PARAMETERS FOR THE ISLAND-WALL INTERACTION AS FUNCTIONS OF THE DEGREE OF WALL STABILIZATION β

β	$(\hat{\omega}_0)_{\text{crit}}$	$(\hat{W}_0)_{\text{crit}}$
1.0	3.0	1.0
0.8	1.81	0.95
0.6	1.12	0.87
0.4	0.82	0.82
0.2	0.65	0.79
0.0	0.56	0.77
-0.2	0.49	0.76
-0.4	0.44	0.74
-0.6	0.40	0.74
-0.8	0.38	0.73
-1.0	0.35	0.72

just sufficient to marginalize the mode at high rotation frequencies; and $\beta = -1$, corresponding to a wall stabilization strong enough to completely stabilize the mode at high frequencies. It can be seen that for $\hat{\omega}_0 < (\hat{\omega}_0)_{\text{crit}}(\beta)$, where the critical value is listed in Table I, there is a continuous spectrum of stable steady state solutions with $\hat{\omega}$ in the range $[0, \hat{\omega}_0]$. However, for $\hat{\omega}_0 > (\hat{\omega}_0)_{\text{crit}}(\beta)$ this spectrum bifurcates into two separate branches. The ‘low drag’ branch is mostly made up of solutions with frequencies of the order of the natural frequency, whilst the ‘high drag’ branch is made up of solutions with much lower frequencies of the order of the inverse wall time constant. A similar bifurcation of solutions is described in Ref. [17]. This bifurcation is a consequence of the non-monotonic variation of the electromagnetic drag torque (42) with the island frequency. At low frequencies the torque is relatively small because the currents induced in the wall are small, at intermediate frequencies (i.e. $\omega\tau_w \sim O(1)$) the torque reaches a maximum, and at high frequencies the torque becomes small again because the rotating magnetic flux is expelled from the wall. Bifurcated ‘low slip’ and ‘high slip’ states are encountered in the analysis of conventional induction motors due to a similar non-monotonic variation of the drag torque with the slip frequency.

As the island width increases, there is a transition from a low drag state with $\omega/\omega_0 \sim 1$ to a high drag state with $\omega/\omega_0 \ll 1$. For $\hat{\omega}_0 < (\hat{\omega}_0)_{\text{crit}}$, the transition is fairly gradual and takes place at $\hat{W}_0 < (\hat{W}_0)_{\text{crit}}(\beta)$, where the critical value is listed in Table I. For $\hat{\omega}_0 = (\hat{\omega}_0)_{\text{crit}}$, the transition is quite abrupt and takes place at about $\hat{W}_0 = (\hat{W}_0)_{\text{crit}}$. For $\hat{\omega}_0 > (\hat{\omega}_0)_{\text{crit}}$, the

low drag and high drag states become separated in mode frequency space by an unstable region for which no stable steady state solutions of Eq. (51) exist. Transitions across the unstable region are presumed to occur when no more stable steady states are available, and take place via a transient process in which inertia, viscosity and the wall drag all play a significant role. In general, it takes of the order of the momentum confinement time-scale to make such a transition. Note that the low drag to high drag transition takes place at a higher value of \hat{W}_0 (i.e. a larger island width) than does the high drag to low drag transition. However, both transitions take place at $\hat{W}_0 > (\hat{W}_0)_{\text{crit}}$. It follows that once a transition has occurred, a significant change in parameters is needed to reverse it. Thus, in thermodynamic terminology, the transitions are *irreversible*.

As the wall stabilization becomes progressively more significant the low drag states are confined to an ever diminishing region of parameter space. For instance, in Fig. 1(b), where wall stabilization is just sufficient to marginalize the mode in the high frequency limit, the low drag states are approximately confined to the region $\omega/\omega_0 \geq 9/10$ for $\hat{\omega}_0 \geq (\hat{\omega}_0)_{\text{crit}}$. If $\beta < 0$, then wall stabilization is strong enough to stabilize the mode for $\hat{\omega} \geq \hat{\omega}_{\text{max}} = \sqrt{-3\beta}$ (see Eq. (47)). In this situation, the low drag branch ceases to exist for $\hat{\omega}_0 \geq \hat{\omega}_{\text{max}}$ (see Fig. 1(c)). Thus, for $\hat{\omega}_0 \geq \hat{\omega}_{\text{max}}$ the analogy of the high drag to low drag transition discussed previously is a high drag to *stable* transition. The reverse transition is feasible, but would probably require a strong transient perturbation of the plasma (e.g. a minor disruption, or a large sawtooth crash) as a trigger.

3.5. Summary

Using the formalism derived in Section 2, the steady rotation frequency of a tearing island interacting with a conducting wall has been calculated. (The major difference between the steady state solutions presented here and the transient solutions presented in Ref. [16] is that plasma viscosity balances the electromagnetic drag torque in the former case, whereas plasma inertia balances the drag torque in the latter case.) The results can be summarized as follows.

For a given natural mode frequency ω_0 there is a ‘resonant’ wall time constant

$$(\tau_w)_{\text{res}} = 2 \left[1 - \left(\frac{r_s}{r_w} \right)^{2m} \right] |\omega_0| \quad (55)$$

at which the drag torque acting on a rotating island is approximately maximum. Note that in an ohmically heated tokamak $|\omega_0| \propto m$ and $\tau_w \propto m^{-1}$. It follows

that a wall time constant that is resonant with one particular tearing mode in the plasma is likely to be approximately resonant with all the other modes. Let $\hat{\tau}_w = \tau_w/(\tau_w)_{\text{res}}$, then for 'small' wall time constants (i.e. $\hat{\tau}_w \ll 1$) the slowing down of the island rotation frequency ω is *continuous* and *reversible* and obeys

$$\frac{\omega}{\omega_0} \approx \frac{1}{1 + (W_0/W_{\text{wall}_a})^4} \quad (56)$$

where W_0 is the zero frequency (i.e. free boundary) saturated island width. For 'large' wall time constants (i.e. $\hat{\tau}_w \gg 1$), the slowing down of the island rotation obeys

$$\frac{\omega}{\omega_0} \approx \frac{1}{2} + \frac{1}{2} \left[1 - \left(\frac{W_\infty}{W_{\text{wall}_b}} \right)^4 \right]^{1/2} \quad (57)$$

where W_∞ is the high frequency (i.e. perfect wall) saturated island width. At $\omega \approx \omega_0/2$ there is a *discontinuous* and *irreversible* transition to a low rotation (i.e. $\omega \sim \tau_w^{-1}$) state. The critical island widths for significant slowing down of mode rotation in the two limits are

$$W_{\text{wall}_a} = \left\{ \left[\left(\frac{r_w}{r_s} \right)^{2m} - 1 \right] / 2\hat{\tau}_w \right\}^{1/4} W_{\text{unlock}} \quad (58a)$$

$$W_{\text{wall}_b} = \left\{ \left[\left(\frac{r_w}{r_s} \right)^{2m} - 1 \right] \hat{\tau}_w / 2 \right\}^{1/4} W_{\text{unlock}} \quad (58b)$$

Note that the critical island width above which significant slowing down of mode rotation occurs is always greater than, or of the order of, the scale island width W_{unlock} (defined in Eq. (74)).

4. INTERACTION OF A TEARING MODE WITH A

STATIC HELICAL MAGNETIC PERTURBATION

4.1. Introduction

Consider the interaction of a general (m, n) tearing mode, resonant inside the plasma on a *single* flux surface of radius r_s , with a *static* (m, n) magnetic perturbation produced by a thin helical winding located outside the plasma at a radius r_c ($r_c > a$). The helical current flowing in the coil (extent r_{c-} to r_{c+} , say) gives rise to a 'jump' in the derivative of the perturbed poloidal magnetic flux $\psi(r)$ across the coil. Thus,

$$\left[r \frac{\partial \psi}{\partial r} \right]_{r_{c-}}^{r_{c+}} = 2m\psi_c \exp \left(i \int^r \omega(t') dt' \right) \quad (59)$$

in the frame of reference of the island, where $\omega(t)$ is the instantaneous island rotation frequency. The coil

current is parametrized by the perturbed poloidal flux in the absence of plasma, ψ_{vac} , where

$$\psi_{\text{vac}}(r) = \psi_c \left(\frac{r}{r_{c-}} \right)^m \quad (60a)$$

for $0 < r < r_{c-}$ and

$$\psi_{\text{vac}}(r) = \psi_c \left(\frac{r}{r_{c+}} \right)^{-m} \quad (60b)$$

for $r_{c+} < r$, in the frame of reference of the coil. Here, ψ_c is the approximately constant value of ψ inside the coil in the absence of plasma.

4.2. The electromagnetic solution in the outer region

Without loss of generality, $\psi(r)$ in the outer region can be split into two parts. The first part, $\psi_{\text{mode}}(r)$, is described in Section 3.2 and represents a magnetic island at the rational surface. The second part, $\psi_{\text{coil}}(r)$, satisfies the cylindrical tearing mode equation (9), the physical boundary conditions (10) and the continuity constraint (11), but is zero in the island region and is subject to the constraint (59) at the coil. In general, ψ_{coil} is zero for $r < r_{s+}$. The function $\psi_{\text{coil}}(r)$ represents the *ideal* MHD response of the plasma to the helical current flowing in the coil.

If the equilibrium plasma current is mainly concentrated inside the rational surface, so that $j_z(r > r_{s+}) \approx 0$, then it is easily demonstrated that

$$\psi_{\text{coil}}(r, t) \approx \Psi_{\text{vac}} \exp \left(i \int^t \omega(t') dt' \right) \times \left[\left(\frac{r}{r_{s+}} \right)^m - \left(\frac{r}{r_{s+}} \right)^{-m} \right] \quad (61a)$$

for $r_{s+} < r < r_c$ and

$$\psi_{\text{coil}}(r, t) \approx \Psi_{\text{vac}} \exp \left(i \int^t \omega(t') dt' \right) \times \left[\left(\frac{r_c}{r_{s+}} \right)^m - \left(\frac{r_c}{r_{s+}} \right)^{-m} \right] \left(\frac{r}{r_c} \right)^{-m} \quad (61b)$$

for $r_c < r$, in the frame of reference of the island, where the finite width of the coil has been neglected. Here, $\Psi_{\text{vac}} \equiv \psi_{\text{vac}}(r_{s+})$.

The 'toroidal' component of the 'sheet' current flowing in the island region due to the presence of the external perturbation (i.e. the helical current at r_s due to ψ_{coil}) is given by

$$\delta J_{z, \text{coil}} \approx 4\pi^2 R_0 \frac{m}{\mu_0} \Psi_{\text{vac}} \exp \left(i \int^t \omega(t') dt' \right) \quad (62)$$

where use has been made of Eq. (12) and the approximations (61a, b). Again, the part of $\delta J_{z,s\text{coil}}$ that is in phase with the reconnected flux Ψ at the rational surface modifies the island stability, whereas the part that is in phase quadrature gives rise to a $j \times B$ torque acting on the island.

The tearing stability index of the mode can be written as

$$\Delta'_s = \Delta'_{\text{mode}} + \Delta'_{\text{coil}} \quad (63)$$

where Δ'_{mode} is the standard stability index for a free boundary tearing mode, described in Section 3.2, and

$$\Delta'_{\text{coil}} r_s \approx 2m \left(\frac{W_{\text{vac}}}{W} \right)^2 \cos \Delta\varphi \quad (64)$$

parametrizes the effect of the external perturbation on the mode stability. Here, use has been made of Eq. (22) and the approximations (61a, b). The island width W satisfies Eq. (37). The 'vacuum' island width W_{vac} is that obtained by superimposing the vacuum coil perturbation ψ_{vac} onto the equilibrium field; thus,

$$W_{\text{vac}} = 4 \left(\frac{R_0 q_s}{B_z} \right)^{1/2} \left| \frac{\Psi_{\text{vac}}}{S_s} \right|^{1/2} \quad (65)$$

The helical phase shift $\Delta\varphi$ between the O points of the plasma and the vacuum islands is given by

$$\Delta\varphi(t) = \int_0^t \omega(t') dt' + \arg(\Psi_{\text{vac}}) - \arg(\Psi) \quad (66)$$

Note that $d\Delta\varphi/dt \equiv \omega(t)$.

The poloidal electromagnetic torque acting on the island is given by

$$T_{\theta\text{EM}s} \approx -4\pi^2 R_0 \frac{m^2}{\mu_0} |\Psi| |\Psi_{\text{vac}}| \sin \Delta\varphi \quad (67)$$

where use has been made of Eq. (13) and the approximation (61).

4.3. Applications

The above results are used to analyse three cases of interest. The first case is the interaction of a locked island with a static magnetic perturbation (see Section 5). The second is the interaction of a rotating island with a static perturbation (see Section 6). The final case considered is the interaction of a suppressed island (i.e. an island that is prevented from entering the non-linear regime) with a static perturbation (see Section 7).

5. INTERACTION OF A LOCKED ISLAND WITH A STATIC HELICAL MAGNETIC PERTURBATION

5.1. Introduction

Consider the interaction of a 'locked' (i.e. $\omega = 0$) island with a static external magnetic perturbation. It is helpful, at this stage, to define the 'fully reconnected' island width W_{full} , which is the steady state locked island width obtained when the phase shift $\Delta\varphi$ between the plasma and vacuum islands is zero. It follows from Eqs (20), (63) and (64) that $W_{\text{full}}(W_{\text{vac}})$ is the real positive root of the transcendental equation

$$\frac{\Delta'_{\text{mode}}(W_{\text{full}}) r_s}{2m} = - \frac{W_{\text{vac}}^2}{W_{\text{full}}^2} \quad (68)$$

If $\Delta'_{\text{mode}}(W)$ is a monotonic decreasing function of the island width W , then a unique real positive root of Eq. (68), with an associated $\Delta'_{\text{mode}}(W_{\text{full}}) < 0$, exists for all (real positive) values of W_{vac} . For a wide range of plasma parameters the above equation predicts $W_{\text{full}} > W_{\text{vac}}$, i.e. the plasma *amplifies* the external perturbation [48, 49]. The amplification factor takes the form

$$\mathcal{Q}(W_{\text{vac}}) \equiv \frac{W_{\text{full}}}{W_{\text{vac}}} = \left(\frac{2m}{-\Delta'_{\text{mode}}(W_{\text{full}}) r_s} \right)^{1/2} \quad (69)$$

The standard offset-linear mode saturation model (see Eq. (43)) yields

$$0 = \kappa f^3 + (1 + \kappa) f^2 - \cos \Delta\varphi \quad (70)$$

$$\mathcal{Q} = (\kappa/\kappa_{\text{crit}})^{1/3}$$

where $f = W/W_{\text{full}}$ is the 'fraction of reconnection', and

$$0 = \delta \kappa^{2/3} + \kappa + 1$$

$$\delta = \left(\frac{\Delta'_{\text{mode}}(0) r_s}{2m} \right) \Big|_{\kappa_{\text{crit}}}^{2/3}$$

$$\kappa_{\text{crit}} = \frac{1}{2m} [\Delta'_{\text{mode}}(0) - \Delta'_{\text{mode}}(W_{\text{vac}})] r_s \quad (71)$$

Here, δ parametrizes the intrinsic stability of the tearing mode, whereas κ parametrizes the degree of saturation of the mode.

The stability parameter $\delta = (\kappa - 1)/\kappa^{2/3}$ is listed as a function of the saturation parameter κ in Table II. It can be seen that $\kappa \ll 1$ if the unperturbed tearing mode is highly stable (i.e. $\delta \ll -1$), that $\kappa = 1$ if the mode is marginally stable and that $\kappa \gg 1$ if the mode is highly unstable (i.e. $\delta \gg +1$).

TABLE II. CRITICAL PARAMETERS FOR THE ISLAND-COIL INTERACTION AS FUNCTIONS OF THE SATURATION PARAMETER κ AND THE STABILITY PARAMETER δ

κ	δ	$\Delta\hat{\varphi}_{\text{unlock}}$ (deg)	g_{max}	$\kappa^{-1/3} g_{\text{max}}^{-1/2}$
0	$-\infty$	45.0	0.50	∞
0.1	-4.18	45.3	0.50	3.03
0.5	-0.79	47.9	0.54	1.71
1.0	0.0	50.8	0.57	1.32
2.0	0.63	55.9	0.63	1.00
3.0	0.96	60.3	0.67	0.85
4.0	1.19	64.0	0.71	0.75
5.0	1.38	67.2	0.74	0.68
10.0	1.94	76.9	0.84	0.51
∞	∞	90.0	1.00	0

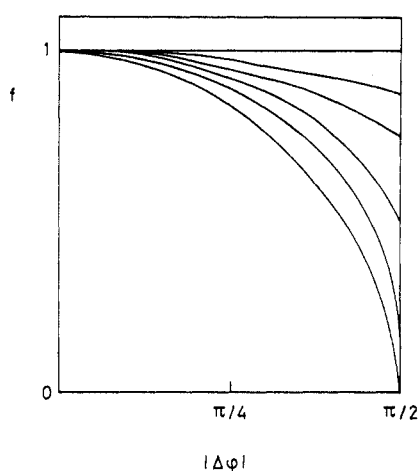


FIG. 2. Fraction of reconnection (f) as a function of the magnitude of the island phase shift ($|\Delta\varphi|$) for a steady state locked island interacting with a static magnetic perturbation, calculated for various different values of the saturation parameter ($\kappa = 0, 1, 2, 4, 8$ and ∞ , where f is a monotonically increasing function of κ).

Figure 2 shows the fraction of reconnection f as a function of the saturation parameter κ and the magnitude of the island phase shift $|\Delta\varphi|$. It can be seen that when the natural mode is stable or close to marginality (i.e. $\kappa \lesssim 1$), f decreases strongly with increasing island phase shift. However, when the natural mode is strongly saturated (i.e. $\kappa \gg 1$), f is only a very weak function of the phase shift. The saturated island width of the unperturbed mode is given by

$$W_0 = \begin{cases} 0 & \kappa \leq 1 \\ \left(1 - \frac{1}{\kappa}\right) W_{\text{full}} & \kappa > 1 \end{cases} \quad (72)$$

5.2. Steady state solutions

For a steady state, the velocity shift profiles in the outer region are again given by Eqs (44a-d), with the associated viscous torque given by Eq. (46). The relationship between the vacuum island width and the steady state island phase shift is obtained from the island equations of motion (31) and the 'no-slip' constraint (24), using Eqs (37), (46a, b), (50), (65) and (67); thus,

$$\frac{(1 - \Gamma)}{\mathcal{Q}^2(\kappa, W_{\text{vac}}) \hat{W}_{\text{vac}}^4} = g(\kappa, \Delta\hat{\varphi}) \equiv f^2(\kappa, \Delta\hat{\varphi}) \sin \Delta\hat{\varphi} \quad (73)$$

in the thin island limit ($W/a \ll 1$), where

$$\Delta\hat{\varphi} = \text{sgn}(\omega_0) \Delta\varphi \quad (74a)$$

$$\Gamma = \frac{\tau_V}{|\omega_0|} \frac{\partial^2 \Delta\hat{\varphi}}{\partial t^2} \frac{W}{r_s} \left[\left(\int_{r_s}^a \frac{\mu_{\perp}(r_s)}{\mu_{\perp}(r')} \frac{dr'}{r'} + \frac{\mu_{\perp}(r_s)}{\mu_{\perp}(a)} \kappa_X \right)^2 + \left(\frac{1}{2} \frac{\delta_D}{r_s} \right)^2 \left(\frac{q_s}{\epsilon_s} \right)^2 \right] \left/ \left[\left(\int_{r_s}^a \frac{\mu_{\perp}(r_s)}{\mu_{\perp}(r')} \frac{dr'}{r'} + \frac{\mu_{\perp}(r_s)}{\mu_{\perp}(a)} \kappa_X \right) + \left(\frac{1}{2} \frac{\delta_D}{r_s} \right) \left(\frac{q_s}{\epsilon_s} \right)^2 \right] \right. \quad (74b)$$

$$\hat{W}_{\text{vac}} = \frac{W_{\text{vac}}}{W_{\text{unlock}}} \quad (74c)$$

$$\frac{W_{\text{unlock}}}{r_s} = \left(\frac{2^8}{m} \mathfrak{F}_{\text{steady}} \frac{\tau_H^2 |\omega_0|}{\tau_V} \right)^{1/4} \quad (74d)$$

The inertia operator Γ is retained in Eq. (73) in order to analyse the stability of solutions. In fact, the solutions are stable provided that

$$\frac{\partial \Delta\hat{\varphi}}{\partial \Gamma} (\Gamma = 0) < 0 \quad (75)$$

that is the system oscillates about the steady state phase shift, rather than exponentiates away from it. Application of Eq. (75) gives the stability criterion

$$\frac{\partial g}{\partial \Delta\hat{\varphi}} > 0 \quad (76)$$

that is the electromagnetic locking torque, which opposes the island phase shift, must increase as the phase shift increases.

The function g is zero when $\Delta\hat{\varphi} = 0$, initially increases with increasing $\Delta\hat{\varphi}$, but reaches a maximum value g_{max} at $\Delta\hat{\varphi}_{\text{unlock}}$ and then starts to decrease with $\Delta\hat{\varphi}$. According to Eq. (76), stable solutions to Eq. (73) are restricted to the region $\Delta\hat{\varphi} < \Delta\hat{\varphi}_{\text{unlock}}$, where $\Delta\hat{\varphi}_{\text{unlock}}(\kappa)$ and $g_{\text{max}}(\kappa)$ are listed in Table II. Note that in all stable states the external perturbation acts so as to increase the island width to some extent (i.e. $\Delta\hat{\varphi} < \pi/2$, see Eqs (20), (63) and (64)). The maximum stable phase

shift is greatest when the unperturbed mode is strongly saturated (i.e. $\kappa \rightarrow \infty$), so that the island width is essentially unaffected by the external perturbation, and smallest when the unperturbed mode is strongly stable (i.e. $\kappa \rightarrow 0$), so that the driven island width decreases with increasing phase shift.

5.3. Mode unlocking

It follows from Eq. (73) that a stable locked island state is only possible when

$$W_{\text{vac}} > (W_{\text{vac}})_{\text{unlock}} \equiv \frac{W_{\text{unlock}}}{Q^{1/2} g_{\text{max}}^{1/4}(\kappa)} \quad (77)$$

The above formula implies that there is a minimum coil current, parametrized by a minimum vacuum island width, required to maintain a locked island in a 'rotating' plasma (i.e. a plasma where the natural mode frequency is non-zero). When $W_{\text{vac}} \gg (W_{\text{vac}})_{\text{unlock}}$, the island locks virtually in phase with the vacuum island (i.e. $\Delta\hat{\phi} \sim 0$). As $W_{\text{vac}} \rightarrow (W_{\text{vac}})_{\text{unlock}}$, a gradually increasing phase shift is set up in the direction of the viscous torque acting on the island. For $W_{\text{vac}} < (W_{\text{vac}})_{\text{unlock}}$, the viscous torque acting on a static island is too large to be balanced by the electromagnetic locking torque, so the island is forced to rotate. The transition from a locked island to a rotating island takes place at $W_{\text{vac}} = (W_{\text{vac}})_{\text{unlock}}$, where the phase shift of the locked island reaches the critical value $\Delta\hat{\phi}_{\text{unlock}}$. This transition is generally referred to as 'mode unlocking'.

The variation of the minimum current ($\propto (W_{\text{vac}})_{\text{unlock}}^2$) with natural mode stability is illustrated in Table II, where $\kappa^{-1/3} g_{\text{max}}^{-1/2}$ (see Eqs (70) and (77)) is tabulated against the stability parameter δ . This is equivalent to scanning $\Delta'_{\text{mode}}(0)$ whilst keeping the gradient of $\Delta'_{\text{mode}}(W)$ (i.e. κ_{crit}) constant. It can be seen that the transition from a highly stable (i.e. $\delta \ll -1$) natural mode, through a marginally stable (i.e. $\delta = 0$) natural mode, to a highly unstable (i.e. $\delta \gg +1$) natural mode is accompanied by a marked reduction in the minimum coil current needed to maintain mode locking.

5.4. Summary

Two asymptotic limits can be identified from the above analysis. In the 'saturated' island limit, the mode is intrinsically highly unstable (i.e. $\delta \gg +1$), so that the island width is essentially unaffected by the external perturbation (i.e. $W = W_0$, where W_0 is the saturated island width). In this limit, a stable locked island state is only possible when

$$W_{\text{vac}} > (W_{\text{vac}})_{\text{unlock}} \equiv \frac{W_{\text{unlock}}^2}{W_0} \quad (78)$$

and the critical island phase shift at unlocking is $\pi/2$. Note from the above that a comparatively large saturated island can be locked by a comparatively weak external perturbation, and vice versa. The crossover point, at which the saturated island is of the same size as the vacuum island needed to lock it, occurs when both island widths are of the order of the scale width W_{unlock} .

In the 'driven' island limit, the mode is intrinsically highly stable (i.e. $\delta \ll -1$), so that the island only exists owing to interaction with the external perturbation. In fact, the driven island width is a strong function of the island phase shift ($W \propto \sqrt{\cos \Delta\hat{\phi}}$). In this limit, a stable locked island state is only possible when

$$W_{\text{vac}} > (W_{\text{vac}})_{\text{unlock}} \equiv \left(\frac{2}{Q}\right)^{1/4} W_{\text{unlock}} \quad (79)$$

and the critical phase shift at unlocking is $\pi/4$. It follows that, in order to maintain a locked island in a strongly tearing-stable plasma, an external perturbation of sufficient amplitude to induce a vacuum island of width greater than, or approximately equal to, the scale width W_{unlock} is required.

The interaction of a non-linear locked island with a static magnetic perturbation is always *destabilizing* (i.e. $\Delta'_{\text{coil}} > 0$, see Eq. (64)).

6. INTERACTION OF A ROTATING ISLAND WITH A STATIC HELICAL MAGNETIC PERTURBATION

6.1. Introduction

An island rotating with an instantaneous (angular) frequency $\omega(t)$ experiences an electromagnetic torque due to interaction with a static external perturbation which modulates like $\sin \Delta\varphi$, where $d\Delta\varphi/dt \equiv \omega(t)$ (see Eq. (67)). The most general solution to Eqs (25a, b), subject to the usual constraints (23a, b), (26) and (28a, b), which displays a similar modulation with the island phase, takes the form

$$\begin{aligned} \Delta\Omega_{\theta}(r, t) = & |\Delta\Omega_{\theta s}| \exp \left[-\cos \left[\frac{1}{2} \tan^{-1}(\omega\tau_D) \right] \right. \\ & \times \left. \left(\frac{1 + \omega^2\tau_D^2}{\omega^2\tau_D^2} \right)^{1/4} \sqrt{|\omega|\tau_V} \frac{|r - r_s|}{r_s} \right] \\ & \times \sin \left[\Delta\varphi - \sin \left[\frac{1}{2} \tan^{-1}(\omega\tau_D) \right] \left(\frac{1 + \omega^2\tau_D^2}{\omega^2\tau_D^2} \right)^{1/4} \right] \end{aligned}$$

$$\times \sqrt{|\omega| \tau_V \frac{|r - r_s|}{r_s} - \varphi_{\text{lag}\theta}} \quad (80a)$$

$$\Delta\Omega_z(r, t) = |\Delta\Omega_{zs}| \exp\left(-\sqrt{\frac{|\omega| \tau_V}{2} \frac{|r - r_s|}{r_s}}\right) \times \sin\left(\Delta\varphi - \text{sgn}(\omega) \sqrt{\frac{|\omega| \tau_V}{2} \frac{|r - r_s|}{r_s}} - \varphi_{\text{lag}z}\right) \quad (80b)$$

in the thin island limit ($W/a \ll 1$), where τ_D is evaluated at the rational surface. The above formulas are valid provided that both the poloidal and 'toroidal' velocity shift profiles are *localized* in the vicinity of the rational surface and any excursions in mode frequency are relatively small. This implies

$$\frac{1}{\sqrt{|\omega| \tau_V}} \ll 1 \quad \left| \frac{1}{\omega^2} \frac{d\omega}{dt} \right| \ll 1 \quad (81)$$

Substitution of Eqs (80a, b) into the island equations of motion (31a, b), making use of Eqs (30) and (67), yields the following expression for the phase lags of the poloidal and 'toroidal' velocity shifts at the rational surface with respect to the driving electromagnetic torque:

$$\varphi_{\text{lag}\theta} = \tan^{-1} \left[\tan\left[\frac{1}{2} \tan^{-1}(\omega \tau_D)\right] + \frac{1}{2} \frac{W}{r_s} \omega \times \left(\frac{\tau_V^2 \tau_D^2}{1 + \omega^2 \tau_D^2} \right)^{1/4} \cos\left[\frac{1}{2} \tan^{-1}(\omega \tau_D)\right] \right] \quad (82a)$$

$$\varphi_{\text{lag}z} = \text{sgn}(\omega) \tan^{-1} \left(1 + \frac{W}{r_s} \sqrt{\frac{|\omega| \tau_V}{2}} \right) \quad (82b)$$

The phase lags are due to a combination of both viscous and inertial effects.

6.2. The viscous limit

6.2.1. The island equation of motion

Viscous effects are dominant in the island-coil interaction when

$$\frac{W}{r_s} \ll \frac{1}{\sqrt{|\omega| \tau_V}} \quad (83)$$

i.e. when the island width is much less than the localization scale length of the 'toroidal' velocity shift profile (see Eqs (80a, b)). In this limit, the island equations of motion (31a, b) can be combined with the no-slip criterion (24) to give the following integral equation which specifies the island phase as a function of time:

$$(1 - \hat{\omega}) \sqrt{\hat{\omega}} = \zeta_1 \sin\left(\Delta\varphi(0) + \int_0^T \hat{\omega}(T') dT' - \varphi_{\text{lag}}\right) \quad (84)$$

where $\hat{\omega} = |\omega/\omega_0|$, $T = |\omega_0|t$, $\zeta_1 = W^2 W_{\text{vac}}^2 / W_{\text{lock}1}^4$,

$$\varphi_{\text{lag}} = \frac{\pi}{4} - \tan^{-1} \left(\frac{\alpha_D \sin \theta_D}{1 + \alpha_D \cos \theta_D} \right) \quad (85a)$$

$$\theta_D = \frac{\pi}{4} - \frac{1}{2} \tan^{-1}(\hat{\omega} |\omega_0| \tau_D) \quad (85b)$$

$$\alpha_D = \left(\frac{q_s}{\epsilon_s} \right)^2 \left(\frac{\hat{\omega}^2 (|\omega_0| \tau_D)^2}{1 + \hat{\omega}^2 (|\omega_0| \tau_D)^2} \right)^{1/4} \quad (85c)$$

$$\frac{W_{\text{lock}1}}{r_s} = \left(\frac{2^9}{m} \mathfrak{F}_{\text{rot}1} \frac{\tau_H^2 \omega_0^2}{\sqrt{\tau_V |\omega_0|}} \right)^{1/4} \quad (85d)$$

$$\mathfrak{F}_{\text{rot}1} = \left(\frac{q_s}{\epsilon_s} \right)^2 \frac{1}{(1 + 2\alpha_D \cos \theta_D + \alpha_D^2)^{1/2}} \quad (85e)$$

Here, $\Delta\varphi(0)$ is the arbitrary phase of the island at $t = 0$, and φ_{lag} is the viscous phase lag of the island frequency shift with respect to the driving electromagnetic torque. The function $\mathfrak{F}_{\text{rot}1}$ parametrizes the effects of poloidal flow damping for non-steady velocity shift profiles.

6.2.2. Solution of the island equations of motion

Equation (84) can be solved by expanding the island frequency as a Fourier series. Thus,

$$\hat{\omega}(T) \simeq \bar{\omega} + \bar{\omega}_1 \cos \bar{\omega} T + \bar{\omega}_3 \cos 3\bar{\omega} T + \dots \quad (86)$$

where $\bar{\omega}$ is the average mode frequency, and $\bar{\omega}_1$, $\bar{\omega}_3$ parametrize periodic oscillations about the average frequency, which are generally known as 'mode locking distortions' [50]. Only the first three terms are retained in the expansion for the sake of simplicity. Equation (84) is only valid in the limit $\bar{\omega}_1/\bar{\omega} \ll 1$, $3\bar{\omega}_3/\bar{\omega} \ll 1$, etc., but this constraint is relaxed close to a rotation frequency maximum or minimum, where $d\omega/dt \simeq 0$ (see the final constraint (81)). The arbitrary phase $\Delta\varphi(0)$ is adjusted so that the minimum frequency in Eq. (86) is coincident with the maximum locking torque in Eq. (84). Thus, $\Delta\varphi(0) = \varphi_{\text{lag}} - \pi/2$.

In the following, the relatively unimportant modulations in φ_{lag} , ζ_1 and $W_{\text{lock}1}$ are time averaged (i.e. $\bar{\omega}$ is substituted for $\hat{\omega}$) for the sake of simplicity.

Equation (86) is matched to Eq. (84) at the minimum and maximum locking torques ($\bar{\omega} T = 0, \pi$, respectively), and also at two intermediate torques ($\bar{\omega} T = \pi/2, 3\pi/2$), to give

$$[1 - \bar{\omega} \pm (\bar{\omega}_1 + \bar{\omega}_3)] \sqrt{\bar{\omega} \mp (\bar{\omega}_1 + \bar{\omega}_3)} \approx \pm \zeta_1 \quad (87a)$$

$$(1 - \bar{\omega}) \sqrt{\bar{\omega}} \approx \zeta_1 \sin\left(\frac{\bar{\omega}_1}{\bar{\omega}} - \frac{1}{3} \frac{\bar{\omega}_3}{\bar{\omega}}\right) \quad (87b)$$

Solutions to Eqs (87a, b) are listed in Table III. For a relatively weak mode locking torque (i.e. $\zeta_1 \ll 1$), the island rotates uniformly at the natural frequency (i.e. $\bar{\omega} = 1$, and $\bar{\omega}_1, \bar{\omega}_3 \rightarrow 0$). As the locking torque gradually increases in strength (i.e. $\zeta_1 \rightarrow O(1)$) the island rotation becomes increasingly non-uniform (i.e. $\bar{\omega}_1, \bar{\omega}_3 \neq 0$) and the average frequency is reduced below the natural frequency (i.e. $\bar{\omega} < 1$). If the locking torque exceeds a critical strength, corresponding to $\zeta_{crit1} = 0.3848$, then the quasi-steady rotating solutions of Eq. (84) break down at low rotation frequency (i.e. below $\hat{\omega} = 1/3$). This behaviour is a consequence of the variation of the viscous torque with mode frequency (see the left hand side of Eq. (84)). The viscous torque is proportional to the frequency shift of the island with respect to the natural frequency (i.e. $\omega_0 - \omega$), but is inversely proportional to the perpendicular velocity length scale ($\propto \omega^{-1/2}$). It follows that the viscous torque attains a maximum value when the island frequency is one third of the natural frequency. Thus, there is a definite limit to the magnitude of the electromagnetic locking torque that can be balanced by a viscous torque in a quasi-steady rotating solution. If the limit is exceeded (i.e. $\zeta_1 \geq \zeta_{crit1}$), then the system is assumed to make a transition to one of the locked island solutions described in Section 5. This transition is generally known as 'mode locking'.

TABLE III. FOURIER COMPONENTS OF THE ROTATION FREQUENCY OF AN ISLAND INTERACTING WITH A STATIC EXTERNAL MAGNETIC PERTURBATION IN THE VISCOUS LIMIT (see Eq. (86))

ζ_1	$\bar{\omega}$	$\bar{\omega}_1$	$\bar{\omega}_3$	$G_1(\zeta_1)$
0.0	1.0	0.0	0.0	0.320
0.05	0.999	0.032	0.018	0.320
0.10	0.995	0.064	0.037	0.320
0.15	0.988	0.097	0.055	0.326
0.20	0.978	0.132	0.075	0.337
0.25	0.964	0.168	0.094	0.347
0.30	0.943	0.212	0.112	0.373
0.35	0.908	0.271	0.126	0.423
0.37	0.891	0.297	0.136	0.446
0.38	0.862	0.337	0.128	0.506
0.3849	0.833	0.379	0.121	0.575

6.2.3. Island stability

Assuming, as is reasonable, that $|\omega| \tau_R \gg 1$, it follows that, to a first approximation, any modulations in Δ'_{coil} (see Eq. (64)) occur on too short a time-scale for the relatively slowly growing island to respond. (In fact, the island width does modulate slightly as the island rotates past the coils, giving rise to a steady electromagnetic torque which acts to slow down the island rotation. This effect is discussed in Section 7.6.) A quasi-steady version of the Rutherford island equation (20) is obtained by averaging over an island rotation period. Thus,

$$I_1 \tau_R(r_s) \frac{d}{dt} \left(\frac{W}{r_s} \right) = \Delta'_{mode}(0) r_s \left(1 - \frac{W}{W_0} \right) + 2m \left(\frac{W_{vac}}{W} \right)^2 \frac{1}{2\pi} \times \oint \cos\left(\Delta\phi(0) + \int_0^T \hat{\omega}(T') dT'\right) d(\bar{\omega}T) \quad (88)$$

where use has been made of Eqs (43), (63) and (64). For a quasi-steady state this reduces to

$$\frac{dW}{dt} \propto 1 - \frac{W}{W_0} - G_1(\zeta_1) \left(\frac{W_{vac}}{W_{lock1}} \right)^4 \left| \frac{\Delta'_{mode}(0) r_s}{2m \sin \varphi_{lag}} \right| = 0 \quad (89)$$

where

$$G_1(\zeta_1) = -\frac{1}{\zeta_1 \pi} \int_0^\pi \cos\left(x + \frac{\bar{\omega}_1}{\bar{\omega}} \sin x + \frac{1}{3} \frac{\bar{\omega}_3}{\bar{\omega}} \sin 3x + \dots\right) dx \quad (90)$$

is listed in Table III. The non-uniform island rotation, which is a consequence of the viscous phase lag (i.e. $\varphi_{lag} > 0$) of the island frequency shift with respect to the modulating locking torque, causes the island to spend a slightly longer time in the stabilizing phase of the external perturbation than in the destabilizing phase. Thus, a rotating island interacting with a static external perturbation experiences a net *stabilizing* effect, in marked contrast to a locked island, which experiences a destabilizing effect. Note that, in general, there is only one quasi-steady solution to Eq. (89), and this is stable to perturbations of the island width.

6.2.4. Mode stabilization versus mode locking

As the coil current ($\propto W_{vac}^2$) is gradually increased, the parameter $\zeta_1 \equiv W^2 W_{vac}^2 / W_{lock1}^4$ initially increases with the vacuum island width W_{vac} , but eventually

reaches a maximum and starts to decrease as the true island width W is reduced via the stabilization mechanism described above (see Eq. (89)). If the maximum value of ζ_1 is less than the critical value $\zeta_{\text{crit}1}$, then the island is *completely stabilized* when the coil current exceeds a critical value parametrized by

$$(W_{\text{vac}})_{\text{stab}} = 1.3 \left(\frac{\Delta'_{\text{mode}}(0)r_s}{2m \sin \varphi_{\text{lag}}} \right)^{1/4} W_{\text{lock}1} \quad (91)$$

where both φ_{lag} and $W_{\text{lock}1}$ are evaluated at $\bar{\omega} = 1$, and use has been made of $G_1(0) = 0.32$ (see Table III). If the maximum value of ζ_1 just equals $\zeta_{\text{crit}1}$, then the mode locks before complete stabilization is achieved when $W = 0.8W_0$. The critical coil current at mode locking is parametrized by

$$(W_{\text{vac}})_{\text{lock}1} = 0.77 \left(\frac{\Delta'_{\text{mode}}(0)r_s}{2m \sin \varphi_{\text{lag}}} \right)^{1/4} W_{\text{lock}1} \quad (92)$$

where both φ_{lag} and $W_{\text{lock}1}$ are evaluated at $\bar{\omega} = 0.833$, and use has been made of $G_1(\zeta_{\text{crit}1}) = 0.575$ (see Table III). If the maximum value of ζ_1 exceed $\zeta_{\text{crit}1}$, then the coil current needed to lock the mode is correspondingly reduced, and $W > 0.8W_0$ when locking occurs. The criterion that the maximum value of ζ_1 lies below $\zeta_{\text{crit}1}$ is equivalent to a limit on the saturated island width:

$$W_0 < (W_0)_{\text{lock}1} = 1.01 \left(\frac{\Delta'_{\text{mode}}(0)r_s}{2m \sin \varphi_{\text{lag}}} \right)^{-1/4} W_{\text{lock}1} \quad (93)$$

where φ_{lag} and $W_{\text{lock}1}$ are evaluated at $\bar{\omega} = 0.833$. If $W_0 < (W_0)_{\text{lock}1}$, then complete mode stabilization is possible, given a sufficiently large coil current, but if $W_0 \geq (W_0)_{\text{lock}1}$, then the mode locks before complete stabilization is achieved.

6.3. The inertial limit

6.3.1. The island equation of motion

Inertia effects are dominant in the island-coil interaction when

$$\frac{W}{r_s} \gg \left(\frac{1 + \omega_0^2 \tau_D^2}{\omega_0^2 \tau_D^2} \right)^{1/4} \frac{1}{\sqrt{|\omega_0| \tau_V}} \quad (94)$$

i.e. when the island width is much greater than the localization scale length of both the poloidal and 'toroidal' velocity shift profiles (see Eqs (80a, b)). In this limit, the integral equation that specifies the island phase as a function of time takes the form

$$(1 - \hat{\omega})\hat{\omega} = \zeta_2 \sin \left(\Delta\varphi(0) + \int_0^T \hat{\omega}(T') dT' - \frac{\pi}{2} \right) \quad (95)$$

where $\hat{\omega} = |\omega/\omega_0|$, $T = |\omega_0|t$, $\zeta_2 = WW_{\text{vac}}^2/W_{\text{lock}2}^3$,

$$\frac{W_{\text{lock}2}}{r_s} = \left(\frac{2^8}{m} \mathfrak{F}_{\text{rot}n_2} \tau_H^2 \omega_0^2 \right)^{1/3} \quad (96a)$$

$$\mathfrak{F}_{\text{rot}n_2} = \left(\frac{q_s}{\epsilon_s} \right)^2 \left[1 + \left(\frac{q_s}{\epsilon_s} \right)^2 \right] \approx 1 \quad (96b)$$

Note that the inertial phase lag of the island frequency shift with respect to the driving electromagnetic torque is $\pi/2$. In the strong poloidal flow damping limit, $\tau_D \rightarrow 0$, the island phase satisfies Eqs (95) and (96a, b) with $\mathfrak{F}_{\text{rot}n_2} \approx (q_s/\epsilon_s)^2$.

6.3.2. Solution of the island equation of motion

Equation (95) can be solved using the Fourier series given in Eq. (86). The solution, which exhibits a behaviour analogous to that of Eq. (84), is listed in Table IV. If the locking torque exceeds a critical strength, corresponding to $\zeta_{\text{crit}2} = 0.25$, then quasi-steady rotating solutions to Eq. (95) break down at low rotation frequencies (i.e below $\hat{\omega} = 1/2$). This behaviour is a consequence of the variation of island inertia with mode frequency (see the left hand side of Eq. (95)). The inertial resistance to shifts in the island frequency is proportional to the amplitude of the frequency shift (i.e. $\omega_0 \rightarrow \omega$) and the instantaneous mode frequency ω . It follows that the inertia attains a maximum value when the island frequency is one half of the natural frequency. Thus, there is a definite limit to the magnitude of the electromagnetic locking torque which can be balanced by inertia in a quasi-steady rotating state. If the limit is exceeded (i.e. $\zeta_2 > \zeta_{\text{crit}2}$) then the system makes a transition to a locked island state.

TABLE IV. FOURIER COMPONENTS OF THE ROTATION FREQUENCY OF AN ISLAND INTERACTING WITH A STATIC EXTERNAL MAGNETIC PERTURBATION IN THE INERTIAL LIMIT (see Eq. (86))

ζ_2	$\bar{\omega}$	$\bar{\omega}_1$	$\bar{\omega}_3$	$G_2(\zeta_2)$	$F(\zeta_2)$
0.0	1.0	0.0	-0.0	0.500	0.0
0.05	0.998	0.050	-0.0001	0.505	0.38
0.10	0.990	0.103	-0.0010	0.520	0.74
0.15	0.974	0.162	-0.0038	0.552	1.04
0.20	0.948	0.236	-0.0118	0.616	1.25
0.23	0.917	0.301	-0.0249	0.703	1.26
0.24	0.900	0.335	-0.0345	0.761	1.21
0.25	0.854	0.423	-0.0700	0.960	1.0

6.3.3. Island stability

The quasi-steady version of the Rutherford island equation, obtained by averaging over an island rotation period, takes the form

$$\frac{dW}{dt} \propto 1 - \frac{W}{W_0} - G_2(\xi_2) \frac{W_{vac}}{W} \times \left(\frac{W_{vac}}{W_{lock_2}} \right)^3 \left| \left(\frac{\Delta'_{mode}(0)r_s}{2m} \right) \right| = 0 \quad (97)$$

where $G_2(\xi_2)$ is listed in Table IV. Again, the non-uniform island rotation, which is a consequence of the inertial phase lag, leads to a net *stabilization* effect.

6.3.4. Mode stabilization versus mode locking

Below a critical saturated island width given by

$$(W_0)_{lock_2} = 0.83 \left(\frac{\Delta'_{mode}(0)r_s}{2m} \right)^{-1/3} W_{lock_2} \quad (98)$$

application of a sufficiently large coil current leads to the disappearance of stable solutions of Eq. (97), with a consequent collapse of the island width to zero on a resistive time-scale. The last stable steady state is characterized by $W = 0.5W_0$. The critical coil current required to induce a collapse is parametrized by

$$(W_{vac})_{coll} = 0.71 \left(\frac{F(\xi_2)\Delta'_{mode}(0)r_s}{2m} \right)^{1/6} W_{lock_2} \quad (99)$$

where $F(\xi_2 = 0.5W_0 W_{vac}^2 / W_{lock_2}^3)$ is listed in Table IV. At $W_0 = (W_0)_{lock_2}$, mode locking takes place prior to any collapse in the island width, when $W = 0.75W_0$. The critical coil current at mode locking is parametrized by

$$(W_{vac})_{lock_2} = 0.63 \left(\frac{\Delta'_{mode}(0)r_s}{2m} \right)^{1/6} W_{lock_2} \quad (100)$$

For $W_0 > (W_0)_{lock_2}$ the critical coil current needed to lock the mode is reduced, and $W > 0.75W_0$ at locking.

6.4. Mode locking versus mode unlocking

A comparison of Eqs (74a-d), (77), (85a-e), (92), (96a, b) and (100) shows that, in general, $(W_{vac})_{lock_1} > (W_{vac})_{unlock}$ and $(W_{vac})_{lock_2} > (W_{vac})_{unlock}$, owing to the reduced velocity shift perpendicular length scale and the consequently increased viscous torque associated with a rotating island state. It follows that once mode locking has occurred and the velocity shift profile has had sufficient time to relax, the coil current must be reduced by a significant amount in order to

induce mode unlocking. Likewise, once mode unlocking has occurred and the system has had sufficient time to reach a quasi-steady state, a significant increase in the coil current is needed to induce mode locking. In thermodynamic terminology, both mode locking and unlocking are *irreversible* processes.

6.5. Summary

The interaction of a rotating non-linear island with a static external perturbation is always *stabilizing*, owing to oscillatory modulations induced in the island frequency, which cause the island to spend slightly more time in the stabilizing phase of the external perturbation than in the destabilizing phase. Mode stabilization is predominantly a viscous effect at small island widths and predominantly an inertial effect at larger island widths. For a sufficiently small unperturbed saturated island width ($W_0 < (W_0)_{lock}$, see Eqs (93) and (98)) the island can be completely stabilized, given a large enough perturbation field strength ($W_{vac} > (W_{vac})_{stab}$ in the viscous regime, $W_{vac} > (W_{vac})_{coll}$ in the inertial regime, see Eqs (91) and (99)). As the saturated island width is increased, the modulations in frequency needed to stabilize the mode become more and more violent. Above a critical saturated island width ($W_0 > (W_0)_{lock}$), conventional mode locking [1, 14, 18] occurs before complete mode stabilization can be achieved.

7. INTERACTION OF A SUPPRESSED ISLAND WITH A HELICAL MAGNETIC PERTURBATION

7.1. Introduction

Under certain circumstances the inner region in the vicinity of the rational surface, where ideal MHD breaks down, effectively reduces to a linear layer.

The major difference between the interaction of a non-linear island with an external magnetic perturbation and the interaction of a linear layer with such a perturbation lies in the boundary condition applied to the perturbed plasma flow in the vicinity of the rational surface. For a non-linear island the perturbed flow is subject to the 'no-slip' constraint, Eq. (24). For a linear layer this constraint is relaxed, although continuity of the perturbed flow across the layer is still a requirement (see Eqs (23a, b)).

The relaxation of the 'no-slip' constraint for a linear layer is implicit in the (single fluid) formalism presented in Section III of Ref. [19]. The basic expansion parameter is

$$\lambda \sim \left(\frac{\delta_{\text{layer}}}{W} \right)^{3/2} \quad (101)$$

where $\delta_{\text{layer}} \sim (\tau_H^2/\tau_V\tau_R)^{1/6}r_s$ is the appropriate linear layer width for an externally driven visco-resistive tearing mode. (Note that owing to an unfortunate typographical error in Ref. [19], λ is mis-spelled γ in its defining equation (82). Furthermore, the simple relationship between λ and the ratio of the linear layer width to the island width is obscured because the inappropriate inviscid layer width is quoted.) Section III of Ref. [19] is only concerned with the non-linear regime ($\lambda \ll 1$). In this regime, expansion of the visco-resistive MHD equations in λ yields a solution in which the flow inside the island separatrix is circulatory in nature, the flow outside the separatrix follows the flux surfaces, and there is no flow across the separatrix (i.e. there is no 'slip'). The flows inside and outside the island separatrix are matched via a viscous boundary layer of thickness similar to that of the linear layer. The non-linear solution is strongly affected by plasma viscosity and inertia, but is only weakly dependent on the plasma resistivity via a $\ln \lambda$ variation of the matching conditions across the separatrix.

In the linear regime ($\lambda \gg 1$), expansion of the visco-resistive MHD equations in λ^{-1} yields a solution in which the non-helical component of the perturbed flow completely decouples from the helical component, becoming independent of the local velocity of the perturbed magnetic field (i.e. the flux surface averaged flow 'slips' with respect to the perturbed field). The helical component of the perturbed flow is localized within the layer and co-rotates with the perturbed magnetic field. In general, the linear solution is dependent on plasma viscosity, inertia and resistivity.

In the following, the 'tearing frequency' is defined as the frequency at which the layer response to a rotating resonant magnetic perturbation is maximal [19] and can be thought of as the rotation frequency of the 'tearing frame'. In the unperturbed plasma the tearing frequency is identical with the natural frequency ω_0 . In a general plasma the tearing frequency is denoted by ω'_0 . The 'no-slip' constraint implies the identity of the tearing frequency and the rotation frequency of the reconnected magnetic flux. Thus, for a non-linear island the tearing frequency is identical with the island rotation frequency.

Strictly speaking, linear analysis is only valid when the predicted island width is much smaller than the linear layer width. However, as soon as a magnetic island enters the non-linear regime it becomes subject to the 'no-slip' constraint, i.e. the tearing frequency must

become identical with the island rotation frequency. If the island is unable to satisfy this constraint it will remain in a 'suppressed' state, with a width of the order of the linear layer width and the plasma flow 'slipping' through it to some extent. The physics of the suppressed island state lies somewhere between the non-linear and linear regimes, but is probably more akin to the linear regime owing to the relaxation of the 'no-slip' constraint. It is conjectured that, to a first approximation, a suppressed island can be treated as a linear layer, so that the analysis presented in this section is valid whenever an island is prevented from entering the non-linear regime. This is an approach which is distinctly different from that taken in Ref. [19], where it was assumed that the dynamics of the suppressed island state is determined by the existence or non-existence of certain non-linear island states.

7.2. Basic theory

For a layer driven by an external perturbation oscillating with a frequency ω_{coil} , asymptotic matching to the two linearly independent outer solutions, ψ_{mode} (described in Section 3.2) and ψ_{coil} (described in Section 4.2), yields

$$\psi_{\text{layer}}(r_{s-}, t) \approx \Psi \exp(-i\omega_{\text{coil}}t) \quad (102a)$$

$$\psi_{\text{layer}}(r_{s+}, t) \approx [\Psi + \psi'_{\text{coil}}(r_s)\delta_{\text{layer}}/2] \exp(-i\omega_{\text{coil}}t) \quad (102b)$$

in the laboratory frame. Here, $r_{s\pm} = r_s \pm \delta_{\text{layer}}/2$, and δ_{layer} is the linear layer width. It follows that

$$\frac{\Psi}{\Psi_{\text{full}}} = \frac{1}{1 + \Delta_{\text{layer}}/(-\Delta'_{\text{mode}})} \quad (103)$$

[19], where Ψ is the perturbed magnetic flux at the edge of the layer,

$$\Psi_{\text{full}} = -\frac{\psi'_{\text{coil}}(r_s)}{\Delta'_{\text{mode}}} \approx -\frac{2m}{\Delta'_{\text{mode}}r_s} \Psi_{\text{vac}} \quad (104)$$

is the 'fully reconnected' magnetic flux (see Section 5.1), Δ'_{mode} is the linear (i.e. zero island width) intrinsic tearing stability parameter of the mode (see Eq. (40)), and Δ_{layer} is determined from the asymptotic behaviour of the layer solution assuming an $\exp(-i\omega_{\text{coil}}t)$ time dependence of layer quantities. Thus, if the perturbed poloidal flux of the layer has the asymptotic form

$$\psi_{\text{layer}}(r_{s-}, t) \approx (b_0 + b_- \delta_{\text{layer}}/2) \exp(-i\omega_{\text{coil}}t) \quad (105a)$$

$$\psi_{\text{layer}}(r_{s+}, t) \approx (b_0 + b_+ \delta_{\text{layer}}/2) \exp(-i\omega_{\text{coil}}t) \quad (105b)$$

in the laboratory frame, then

$$\Delta_{\text{layer}} = \frac{b_+ - b_-}{b_0} \quad (106)$$

Note that for a linear layer the rotation frequency of the reconnected magnetic flux is that imposed by the external perturbation. The phase shift of the reconnected magnetic flux Ψ at the edge of the layer with respect to the vacuum flux is given by

$$\begin{aligned} \Delta\varphi &= \arg(\Psi_{\text{vac}}) - \arg(\Psi) \\ &= \tan^{-1} \left(\frac{\text{Im}(\Delta_{\text{layer}}/|\Delta'_{\text{mode}}|)}{1 + \text{Re}[\Delta_{\text{layer}}/(-\Delta'_{\text{mode}})]} \right) \end{aligned} \quad (107)$$

(see Eqs (18) and (19)).

The electromagnetic torque exerted on the plasma in the vicinity of the layer satisfies

$$T_{\theta\text{EM}} = 4\pi^2 R_0 \frac{m}{\mu_0} \frac{i}{4} \left[r \frac{\partial \psi}{\partial r} \psi^* - r \frac{\partial \psi^*}{\partial r} \psi \right]_{r_s^-}^{r_s^+} \quad (108)$$

This is a slightly more general formula than that of Eq. (13), which is only valid when the ‘constant ψ ’ approximation holds. Note that the torque only depends on the asymptotic behaviour of the layer solution. The above equations imply that

$$T_{\theta\text{EM}} \approx -4\pi^2 R_0 \frac{m^2}{\mu_0} |\Psi| |\Psi_{\text{vac}}| \sin \Delta\varphi \quad (109)$$

(see Eq. (67)). Thus, if the phase shift $\Delta\varphi$ is non-zero the external coil exerts a steady (i.e. non-modulating) electromagnetic drag torque on the plasma in the vicinity of the rational surface.

The electromagnetic drag torque acting in the vicinity of the rational surface modifies the bulk plasma rotation, shifting the tearing frequency by

$$\Delta\omega_0 = \omega'_0 - \omega_0 = m\Delta\Omega_{\theta s} - n\Delta\Omega_{z s} \quad (110)$$

where ω_0 is the original tearing frequency (i.e. the natural frequency) and ω'_0 is the new tearing frequency, and $\Delta\Omega_{\theta s}$ and $\Delta\Omega_{z s}$ are the components of the phenomenological single fluid velocity shift in the vicinity of the rational surface (see Section 2.5). The steady state velocity shift profiles in the outer region are given by Eqs (44a-d). The associated steady viscous torque exerted on the plasma in the vicinity of the rational surface is given by Eqs (46a, b).

7.3. Linear layer physics

The single fluid linear layer equations, assuming an $\exp(-i\omega_{\text{coil}}t)$ time dependence of layer quantities and a modified bulk plasma rotation, take the form

$$i \frac{d^2\psi}{dy^2} = -\Delta\omega\tau_R(\psi - y\phi) \quad (111a)$$

$$y \frac{d^2\psi}{dy^2} = (\Delta\omega)^2\tau_H^2 \frac{d^2\phi}{dy^2} + i \frac{\Delta\omega\tau_H^2}{\tau_V} \frac{d^4\phi}{dy^4} \quad (111b)$$

[39], where ψ is the perturbed poloidal flux, $\phi = s(r_s)B_\theta(r_s)\xi$ (s is the magnetic shear and B_θ is the equilibrium poloidal magnetic field), ξ is the plasma displacement, $y = r/r_s$, and $\Delta\omega \equiv \omega'_0 - \omega_{\text{coil}}$ is the ‘slip frequency’ between the tearing frame and the reconnected magnetic flux. The time-scales τ_R , τ_H and τ_V are defined in Eqs (21) and (52f, g).

Consider the limit $\tau_R \gg \tau_V$, which is appropriate to most tokamak plasmas, except close to the edge of discharges. Three distinct subsidiary limits can be identified as the slip frequency is varied. In the first limit, viscosity and resistivity are of equal importance in the layer, whereas inertia is unimportant. In this visco-resistive limit, $|\Delta\omega| \ll \omega_{I_1} \equiv \tau_V^{1/3}/\tau_H^{2/3}\tau_R^{2/3}$ and

$$\frac{\delta_{\text{layer}}}{r_s} \sim \frac{\tau_H^{1/3}}{\tau_R^{1/6}\tau_V^{1/6}} \quad (112a)$$

$$\Delta_{\text{layer}} r_s = 2.1036\Delta\omega \left(\frac{\tau_H^{1/3}\tau_R^{5/6}}{\tau_V^{1/6}} \right) \exp(i\pi/2) \quad (112b)$$

In the second limit, viscosity alone is important in the layer. In this ideal viscous limit,

$$\omega_{I_1} \ll |\Delta\omega| \ll \omega_{I_2} \equiv 1/\tau_H^{2/3}\tau_V^{1/3}$$

and

$$\frac{\delta_{\text{layer}}}{r_s} \sim \frac{|\Delta\omega|^{1/4}\tau_H^{1/2}}{\tau_V^{1/4}}$$

$$\Delta_{\text{layer}} r_s = \frac{4.6475}{|\Delta\omega|^{1/4}} \left(\frac{\tau_V^{1/4}}{\tau_H^{1/2}} \right) \exp[\text{isgn}(\Delta\omega)7\pi/8] \quad (113)$$

Finally, in the third limit, inertia alone is important in the layer. In this ideal inertial limit, $\omega_{I_2} \ll |\Delta\omega|$ and

$$\frac{\delta_{\text{layer}}}{r_s} \sim |\Delta\omega|\tau_H \quad (114a)$$

$$\Delta_{\text{layer}} r_s = \frac{\pi}{\Delta\omega\tau_H} \exp(i\pi/2) \quad (114b)$$

The ‘constant ψ ’ approximation is valid whenever

$$|\Delta\omega|\tau_R \left(\frac{\delta_{\text{layer}}}{r_s} \right)^2 \ll 1 \quad (115)$$

(see Eqs (111a, b)). It follows from the above that the ‘constant ψ ’ approximation holds in the visco-resistive limit, but is invalid in the two ideal limits. The breakdown of the ‘constant ψ ’ approximation in the ideal limit is not surprising, since if resistivity is neglected in the layer equations (111a, b) then there is zero

reconnected flux at the centre of the layer even when the flux at the edge is non-zero.

In the visco-resistive limit the reconnected flux Ψ given rise to a standard 'constant ψ ' magnetic island whose width is proportional to $|\Psi/B_z|^{1/2}$ (see Eq. (37)). In the ideal limit there is no change in topology of the magnetic flux surfaces, although the perturbed flux at the edge of the layer Ψ can be non-zero.

7.4. The visco-resistive limit

7.4.1. Introduction

Consider the case of a static external perturbation (i.e. $\omega_{\text{coil}} = 0$). If the natural mode frequency ω_0 is much less than ω_{I_1} then the layer always remains in the visco-resistive limit (see Section 7.3). In this limit, the typical reconnection time-scale is given by

$$\tau_{\text{rec}} = \frac{2.1036}{|\Delta'_{\text{mode}} r_s|} \frac{\tau_H^{1/3} \tau_R^{5/6}}{\tau_V^{1/6}} \quad (116)$$

Equations (103), (107) and (112a, b) yield

$$\left| \frac{\Psi}{\Psi_{\text{full}}} \right| = \frac{1}{(1 + 3\hat{\omega}^2)^{1/2}} \quad (117a)$$

$$\Delta\phi = \tan^{-1}(\sqrt{3}\hat{\omega}) \quad (117b)$$

where $\hat{\omega} = \omega_0 \tau_{\text{rec}} / \sqrt{3}$ is the slip frequency normalized with respect to the typical reconnection time-scale. It follows that if the slip frequency is less than, or of the order of, the inverse reconnection time-scale, a relatively large amount of reconnection is driven, and the island phase shift with respect to the vacuum island is significantly less than $\pi/2$. However, if the slip frequency is much greater than the inverse reconnection time-scale, very little reconnection is driven and the island phase shift approaches $\pi/2$ asymptotically. This phase shift is due to the viscous drag exerted on the island by the flowing plasma and is in the direction of the rotation of the tearing frame.

According to Eqs (109) and (117a, b) the electromagnetic drag torque acting in the vicinity of the rational surface is given by

$$T_{\theta\text{EM}} \cong -4\pi^2 R_0 \frac{m^2}{\mu_0} \frac{2m}{|\Delta'_{\text{mode}} r_s|} \frac{\sqrt{3}\hat{\omega}}{1 + 3\hat{\omega}^2} |\Psi_{\text{vac}}|^2 \quad (118)$$

Note that this torque is almost identical in form with the drag torque acting on a rotating island interacting with a resistive wall (see Eq. (42)), with the slip frequency taking the place of the island frequency, the layer reconnection time-scale taking the place of the wall time constant, and the vacuum magnetic flux taking

the place of the reconnected flux [24]. This effect is a special property of the visco-resistive layer and does not occur in other limits.

7.4.2. The steady state tearing frequency

The relation between the steady state slip frequency $\hat{\omega}'_0$ and the natural frequency ω_0 is obtained from the island equations of motion (31a, b), using Eqs (46a, b), (50), (110) and (118); thus,

$$\hat{\omega}'_0 = \hat{\omega} \left(1 + \frac{8\hat{W}_{\text{vac}}^4}{(1 + 3\hat{\omega}^2)} \right) + \Gamma \quad (119)$$

where

$$\begin{aligned} \Gamma = \tau_V \frac{\partial \hat{\omega}}{\partial t} \frac{\delta_{\text{layer}}}{r_s} \left[\left(\int_{r_s}^a \frac{\mu_{\perp}(r_s)}{\mu_{\perp}(r')} \frac{dr'}{r'} + \frac{\mu_{\perp}(r_s)}{\mu_{\perp}(a)} \kappa_X \right)^2 \right. \\ \left. + \left(\frac{1}{2} \frac{\delta_D}{r_s} \right)^2 \left(\frac{q_s}{\epsilon_s} \right)^2 \right] / \left[\left(\int_{r_s}^a \frac{\mu_{\perp}(r_s)}{\mu_{\perp}(r')} \frac{dr'}{r'} + \frac{\mu_{\perp}(r_s)}{\mu_{\perp}(a)} \kappa_X \right) \right. \\ \left. + \left(\frac{1}{2} \frac{\delta_D}{r_s} \right) \left(\frac{q_s}{\epsilon_s} \right) \right] \quad (120a) \end{aligned}$$

$$\hat{\omega}'_0 = \omega_0 \tau_{\text{rec}} / \sqrt{3} \quad (120b)$$

$$\hat{W}_{\text{vac}} = W_{\text{vac}} / W_{\text{rec}} \quad (120c)$$

$$\frac{W_{\text{rec}}}{r_s} = \left(\frac{2^{11}}{m} \mathfrak{S}_{\text{steady}} \frac{|\Delta'_{\text{mode}} r_s|}{2m} \frac{\tau_H^2}{\tau_{\text{rec}} \tau_V} \right)^{1/4} \quad (120d)$$

Note the similarity between Eq. (119), which describes the slowing down of the rotation of the tearing frame due to interaction with a static external perturbation, and Eq. (51), which describes the slowing down of the rotation of a magnetic island interacting with a resistive wall.

The inertia operator Γ is retained in Eq. (119) in order to analyse the stability of solutions. In fact, the solutions are stable, provided that

$$\frac{\partial \hat{\omega}}{\partial \Gamma} (\Gamma = 0) < 0 \quad (121)$$

which reduces to

$$\frac{6\hat{\omega}^3}{1 - 3\hat{\omega}^2} + \hat{\omega}'_0 < 0 \quad (122)$$

Now, a suppressed island can enter the non-linear regime as soon as it is able to satisfy the 'no-slip' constraint (i.e. $\omega'_0 = 0$, for a static perturbation) whilst remaining in a stable torque balance. For the case under consideration this occurs when

$$\hat{\omega}'_0 < \frac{\hat{\omega}(1 + 3\hat{\omega}^2)}{(\sqrt{3}\hat{\omega} - 1)^2} \quad (123)$$

for $\hat{\omega} < 1/\sqrt{3}$, where the variation of Δ'_{mode} with island

width has been neglected (i.e. $\kappa = 0$ in the notation of Section 5.1). The non-linear island states at the boundary between the linear and non-linear regimes all have phase shifts of $\pi/4$ with respect to the vacuum island, which is the maximum stable phase shift achievable in the non-linear regime (for $\kappa = 0$) (see Section 5.2 and Table II).

7.4.3. Description of the steady state solution

Figure 3 shows steady state solutions of Eq. (119) plotted as contours of constant \hat{W}_{vac} (normalized vacuum island width or normalized perturbation field strength) in the $\hat{\omega}$ (normalized slip frequency) versus $\hat{\omega}_0$ (normalized natural frequency) plane. The boundary between stable and unstable solutions and the extent of the non-linear regime are also indicated.

It can be seen from Fig. 3 that application of an external perturbation modifies the bulk plasma rotation (this is parametrized by a reduction in the slip frequency). If the natural frequency lies below a critical value, given by $(\omega_0)_{\text{crit}} = 3\sqrt{3}/\tau_{\text{rec}}$ (i.e. effectively the inverse layer reconnection time-scale), then there is a continuous spectrum of stable slipping states between the unperturbed state and the first accessible non-linear state.

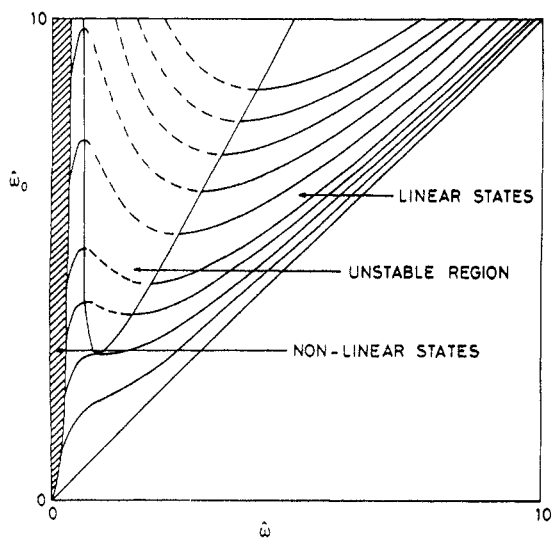


FIG. 3. Steady state solutions for the interaction of a visco-resistive tearing layer with a static magnetic perturbation. Contours of constant normalized vacuum island width (\hat{W}_{vac}) are plotted in the normalized tearing frequency ($\hat{\omega}$) versus normalized natural frequency ($\hat{\omega}_0$) plane. Dashed contours denote unstable solutions. The hatched region represents the extent of non-linear solutions. The contours plotted are $\hat{W}_{\text{vac}}^{1/4} = 0.0, 0.5, 1.0, 1.5, 2.0, 3.0, 4.0, 5.0, 6.0$ and 7.0 (the contours are crossed, in the listed order, as $\hat{\omega}_0$ is increased from zero at constant $\hat{\omega}$).

Thus, the transition between the unreconnected state and the fully reconnected state is achieved in a *continuous* and *reversible* manner as the external perturbation strength is gradually increased from zero. This transition is associated with a gradual change in the bulk plasma rotation, with an associated gradual reduction of the slip frequency from the unperturbed value ω_0 to zero in the non-linear regime.

If the natural frequency lies above the critical value $(\omega_0)_{\text{crit}}$, then some of the intermediate slipping states become unstable. Thus, when the amplitude of the external perturbation is raised above a certain critical value, the system crosses the high slip boundary of the unstable region and makes a transition to a stable solution on the low slip side. The unstable region is only encountered when $W_{\text{vac}} > W_{\text{rec}}$ (see Eqs (120a-d)). The transition is characterized by an abrupt increase in the reconnected magnetic flux and an abrupt change in the bulk plasma rotation. In general, it takes a time of the order of the momentum confinement time-scale to complete a transition over the unstable region. The reverse transition occurs when the system crosses the low slip boundary of the unstable region. For fixed ω_0 , this occurs at a somewhat lower external perturbation field strength than that required to trigger the high rotation to low rotation transition (see Fig. 3). It follows that if the natural frequency ω_0 lies above the critical value $(\omega_0)_{\text{crit}}$, then the transition from the unreconnected state to the fully reconnected state is neither continuous nor reversible.

7.4.4. Mode penetration

In the asymptotic limit where the unperturbed natural frequency is much greater than the inverse layer reconnection time-scale, the slowing down of plasma rotation due to interaction with the external perturbation is parametrized by

$$\frac{\omega'_0}{\omega_0} \approx \frac{1}{2} + \frac{1}{2} \left[1 - \left(\frac{W_{\text{vac}}}{W_{\text{pen}_1}} \right)^4 \right]^{1/2} \quad (124)$$

where

$$\frac{W_{\text{pen}_1}}{r_s} = \left(\frac{67.31}{m^2} \mathfrak{J}_{\text{steady}} \omega_0^2 \frac{\tau_H^{7/3} \tau_R^{5/6}}{\tau_V^{7/6}} \right)^{1/4} \quad (125)$$

Thus, as the perturbation strength is gradually increased the slip frequency is gradually decreased until it reaches one half of its original value, at which point the system makes an irreversible transition to a non-linear island state. Such a transition is generally referred to as 'mode penetration' [22, 23], and is characterized by an abrupt and sizeable increase in the reconnected magnetic flux,

with a simultaneous abrupt change in the bulk plasma rotation. Mode penetration is distinguished from mode locking (described in Section 6) by the absence of any rotating island state immediately prior to the production of the non-linear locked island state. Mode locking is essentially a transition from a rotating island state to a locked island state and is brought about by the slowing down and eventual locking of the island rotation. Mode penetration, on the other hand, is a transition from a suppressed (but locked) island state to an unsuppressed (but locked) island state and is brought about by the slowing down and eventual locking of the rotation of the tearing frame.

Mode penetration takes place when the vacuum island width exceeds the critical value W_{pen1} (see Eqs (124) and (125)), which is a function of the plasma resistivity and viscosity. The predicted scaling of the critical perturbed field strength required to induce mode penetration is $\delta B \sim \tau_H |\omega_0| S^{5/12} \nu^{7/12}$ (where $S = \tau_R/\tau_H$ and $\nu = \tau_H/\tau_V$), which is in good agreement with a previous numerical study of penetration [25].

The process inverse to mode penetration is mode unlocking (described in Section 5). As long as the island remains in the non-linear regime its rotation frequency is tied to that of the tearing frame via the 'no-slip' constraint. Thus, if the perturbation field strength is reduced in order to make the island unlock, both the tearing frame and the island are simultaneously 'spun up' by the viscous torque acting in the vicinity of the rational surface. Only after the island width has decayed back to a width of the order of the linear layer width is the 'no-slip' constraint relaxed, allowing the island to decouple from the rotating tearing frame and revert to the suppressed (locked) island state.

7.5. The ideal limits

If the natural mode frequency ω_0 is much greater than $\omega_{I1} \equiv \tau_V^{1/3}/\tau_H^{2/3}\tau_R^{2/3}$ then the layer is initially in one of the ideal limits. Figure 4 is a schematic diagram of the variation of the electromagnetic torque ($\propto |\Psi| \sin \Delta\phi$, see Eq. (109)) as a function of the slip frequency ω'_0 , for a fixed amplitude static external magnetic perturbation. The torque is zero when $\omega'_0 = 0$, because the phase shift $\Delta\phi = 0$, and initially rises rapidly with increasing ω'_0 as the phase shift increases, reaching a maximum at $\omega'_0 = \tau_{rec}^{-1}$. As ω'_0 is raised further, the torque falls off approximately like $1/\omega'_0$ as resistive reconnection becomes less efficient, until the boundary between the resistive and ideal regimes is reached at $\omega'_0 \sim \omega_{I1}$. At this point the torque is a minimum. Any further increase in ω'_0 leads to a rising

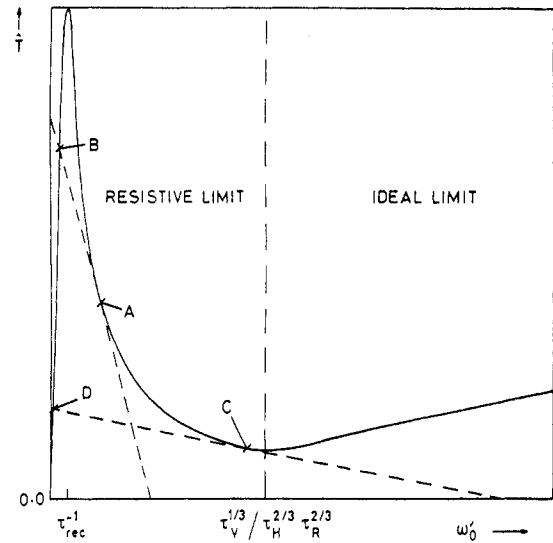


FIG. 4. Schematic diagram of the normalized electromagnetic torque (\hat{T}) exerted by a static external magnetic perturbation at fixed amplitude on the plasma in the vicinity of a tearing layer, calculated as a function of the slip frequency between the tearing frame and the reconnected magnetic flux (ω'_0). Balance points between the electromagnetic and viscous torques acting in the vicinity of the rational surface correspond to the intersection of the torque curve with a straight line of negative gradient which passes through $\omega'_0 = \omega_0$ at $\hat{T} = 0$. Here, ω_0 is the natural mode frequency. Two example straight lines are shown. The first corresponds to visco-resistive mode penetration (i.e. the transition A to B), the second to ideal mode penetration (i.e. the transition C to D).

torque as the layer becomes increasingly ideal in nature, and viscosity and inertia become relatively more important. In the ideal viscous limit the torque increases like $(\omega'_0)^{1/4}$, whereas in the ideal inertial limit it increases like ω'_0 (see Eqs (113) and (114a, b)).

The balance points between the electromagnetic and viscous torques acting in the vicinity of the rational surface correspond to the intersections of the torque curve with a straight line that passes through ω_0 (the natural frequency) at zero torque and has a negative gradient proportional to W_{vac}^{-4} . The balance points are stable if the line passes from above to below the torque curve as ω'_0 increases, and they are unstable if the opposite is the case.

Two example lines are shown in Fig. 4. For the first line, $\omega_0 \ll \omega_{I1}$, so that the layer is always in the visco-resistive limit. The system is just about to make a transition from a stable high slip state (marked A) to a stable low slip state (marked B). This corresponds to a state on the high slip boundary of the unstable region in Fig. 3. The transition (i.e. mode penetration) occurs when $\omega'_0 \sim \omega_0/2$. For the second line, $\omega_0 \gg \omega_{I1}$, so that

the layer is initially in the ideal limit. The system is again just about to make a transition from a stable high slip state (marked C) to a stable low slip state (marked D). The transition (i.e. mode penetration) occurs when the tearing frequency has been reduced to about ω_{I_1} , so that the layer is just about to become resistive and the torque is a minimum.

In the ideal viscous limit the modification of plasma rotation due to interaction with the external perturbation is parametrized by

$$\left(\frac{\omega_0}{\omega'_0}\right)^{1/4} \left(1 - \frac{\omega'_0}{\omega_0}\right) - \left(\frac{W_{\text{vac}}}{W_{\text{slow}_1}}\right)^4 = 0 \quad (126)$$

where

$$\frac{W_{\text{slow}_1}}{r_s} = \left(\frac{1.55 \times 10^3}{m^2} \mathfrak{J}_{\text{steady}} \frac{|\omega_0|^{3/4} \tau_H^{3/2}}{\tau_V^{3/4}}\right)^{1/4} \quad (127)$$

Mode penetration occurs when $\omega'_0 \sim \omega_{I_1}$ or when $W_{\text{vac}} \geq W_{\text{pen}_2}$, where

$$\frac{W_{\text{pen}_2}}{r_s} \sim \left(\frac{67.31}{m^2} \mathfrak{J}_{\text{steady}} |\omega_0| \frac{\tau_H^{5/3} \tau_R^{1/6}}{\tau_V^{5/6}}\right)^{1/4} \quad (128)$$

The constant in the above formula is chosen such that $W_{\text{pen}_1} = W_{\text{pen}_2}$ when $\omega'_0 = \omega_{I_1}$ (see Eq. (125)). The predicted scaling of the critical perturbed field strength required to induce mode penetration in the ideal limit is $\delta B \sim (\tau_H |\omega_0|)^{1/2} S^{1/12} \nu^{5/12}$.

Finally, in the ideal inertial limit the modification of plasma rotation due to interaction with the external perturbation is parametrized by

$$\frac{\omega'_0}{\omega_0} = \frac{1}{1 + (W_{\text{vac}}/W_{\text{slow}_2})^4} \quad (129)$$

where

$$\frac{W_{\text{slow}_2}}{r_s} = \left(\frac{402.1}{m^2} \mathfrak{J}_{\text{steady}} \frac{\tau_H}{\tau_V}\right)^{1/4} \quad (130)$$

7.6. The non-linear analogue to mode penetration

Consider the case of a non-linear magnetic island of width W , rotating uniformly with a frequency ω . The Rutherford island equation takes the form

$$I_1 \tau_R \frac{d}{dt} \left(\frac{W}{r_s}\right) = \Delta'_{\text{mode}}(W) r_s + 2m \left(\frac{W_{\text{vac}}}{W}\right)^2 \cos \Delta \varphi \quad (131)$$

where $d\Delta\varphi/dt = \omega$. Let

$$W = W^{(0)} + W^{(1)} \sin \Delta \varphi \quad (132)$$

where $W^{(0)}$ is the steady island width. It follows that

$$\frac{W^{(1)}}{r_s} \approx \frac{2m}{I_1 \omega \tau_R} \left(\frac{W_{\text{vac}}}{W^{(0)}}\right)^2 \quad (133)$$

assuming $|W^{(1)}/W^{(0)}| \ll 1$ and neglecting any oscillations in $\Delta_{\text{layer}}(W)$. According to Eq. (133), as the island rotates past the external coils its width modulates slightly under the influence of finite plasma resistivity. The reconnected magnetic flux is written as

$$\Psi = \Psi^{(0)} + \Psi^{(1)} \sin \Delta \varphi \quad (134)$$

in the island frame, where $\Psi^{(0)}$ is the steady state component and $\Psi^{(1)}$ is the amplitude of the modulating component. It is easily demonstrated that

$$\frac{\Psi^{(1)}}{\Psi^{(0)}} = 2 \frac{W^{(1)}}{W^{(0)}} \quad (135)$$

It follows from Eq. (67) that the modulations in the rotating island width give rise to a non-oscillating electromagnetic torque, which acts to slow down the island rotation. The time averaged poloidal component of this torque takes the form

$$T_{\theta \text{EM}} = -4\pi^2 R_0 \frac{m^2}{\mu_0} \frac{2m}{I_1 \omega \tau_R W^{(0)}/r_s} |\Psi_{\text{vac}}|^2 \quad (136)$$

The change in the island induced by the steady electromagnetic drag, obtained in the usual manner by balancing the electromagnetic and viscous torques at the rational surface, is described by

$$\frac{\omega}{\omega_0} = \frac{1}{2} + \frac{1}{2} \left[1 - \left(\frac{W_{\text{vac}}}{W_{\text{lock}_3}}\right)^4\right]^{1/2} \quad (137)$$

where

$$\frac{W_{\text{lock}_3}}{r_s} = \left(\frac{26.33}{m^2} \mathfrak{J}_{\text{steady}} \omega_0^2 \frac{\tau_H^2 \tau_R}{\tau_V} \frac{W^{(0)}}{r_s}\right)^{1/4} \quad (138)$$

The last steady state solution of Eq. (137) occurs when the island frequency has been reduced to one half of its original value, that is when $W_{\text{vac}} = W_{\text{lock}_3}$. If $W_{\text{vac}} > W_{\text{lock}_3}$, the electromagnetic drag torque is too large to be balanced by the viscous restoring torque, and the system makes a transition to one of the locked island states discussed in Section 5.

Note the similarity between Eq. (124), which describes the slowing down of plasma rotation due to interaction with an external perturbation in the linear regime, and Eq. (137), which describes the equivalent slowing down of plasma rotation in the non-linear regime. In fact, W_{lock_3} can be re-written as

$$W_{\text{lock}_3} = \left(\frac{W^{(0)}}{\delta_{\text{layer}}}\right)^{1/4} W_{\text{pen}_1} \quad (139)$$

(see Eq. (125)), where $\delta_{\text{layer}}/r_s = 2.56 \tau_H^{1/3} / \tau_R^{1/6} \tau_V^{1/6}$ is the appropriate linear layer width (see Eq. (112a)). It

follows that the mode locking mechanism described above is the non-linear analogue of visco-resistive mode penetration. Since the non-linear island width is always greater than the linear layer width, Eq. (139) implies that the external perturbation field strength required to lock a rotating island exceeds that needed to induce mode penetration in an otherwise equivalent tearing-stable plasma.

Note that in describing the steady electromagnetic drag torque associated with modulations in the rotating island *width*, any modulations in the island *frequency*, such as those described in Section 6, have been neglected. Likewise, modulations in the rotating island width are neglected in Section 6. These two effects, which in reality occur simultaneously, have been treated separately for the sake of clarity.

7.7. Summary

An island that is unable to satisfy the ‘no-slip’ constraint is prevented from entering the non-linear regime and remains in a ‘suppressed’ state, with a width of the order of the linear layer and with the plasma slipping through it to some extent. Suppressed islands are most likely to occur during the interaction of an external magnetic perturbation with a tearing-stable plasma. It is assumed that the physics of a suppressed island state is similar to that of a linear layer.

For a linear layer interacting with a static external magnetic perturbation the reconnected flux at the rational surface is non-rotating. The external perturbation exerts a steady electromagnetic drag torque in the vicinity of the rational surface, which modifies the bulk plasma rotation. The amount of driven reconnection is a highly non-linear function of the perturbation field strength (parametrized by the vacuum island width). As the vacuum island width is gradually increased from zero, the modification of plasma rotation gradually increases in strength, but relatively little reconnection is driven at the rational surface. However, above a critical vacuum island width ($W_{\text{vac}} > W_{\text{pen}_1}$ if the layer is resistive, $W_{\text{vac}} > W_{\text{pen}_2}$ if the layer is ideal, see Eqs (125) and (128)), there is an abrupt increase in the reconnected flux as a locked non-linear island is induced at the rational surface. There is a simultaneous abrupt change in the plasma rotation as the rotation of the tearing frame is arrested. This process is known as ‘mode penetration’ [22, 29] and is distinguished from mode locking by the absence of any rotating island state immediately prior to the production of the locked mode.

If the natural frequency is smaller than the inverse layer reconnection time-scale, then the transition to the

locked island state becomes completely smooth and reversible as the perturbed field strength is gradually increased.

The interaction of a rotating island with an external magnetic perturbation can also give rise to a steady electromagnetic drag torque acting in the vicinity of the rational surface. This torque is associated with periodic modulations in the island width. The torque acts to slow down the island rotation, but once a critical vacuum island width is exceeded ($W_{\text{vac}} > W_{\text{lock}_3}$, see Eq. (138)) conventional mode locking occurs. This effect is the non-linear analogue of mode penetration. In fact, the critical perturbation field strength needed to induce locking merges with the critical field strength required to induce penetration as the island width is reduced to that of the linear layer (see Eq. (129)).

8. IMPLICATIONS FOR OHMICALLY HEATED TOKAMAKS

The aim of this section is to make some quantitative predictions for ohmically heated tokamaks, using some of the results derived in Sections 3–7. It is not intended to perform a detailed comparison of theory and experiment, since this is best left to experimental papers, but rather to indicate which of the many effects described in the preceding sections are likely to be of significance in tokamak plasmas. Of particular interest is the scaling of the various effects with machine size.

Consider a family of tokamaks of constant aspect ratio $a = 0.35R_0$, in which the toroidal field strength scales like $B_\phi = 1.38R_0^{0.7}$ T. Broadly speaking, most modern tokamaks of conventional design are members of this family; for instance, COMPASS-C ($R_0 = 0.56$ m, $a = 0.2$ m, $B_\phi = 1.1$ T) [29], DIII-D ($R_0 = 1.67$ m, $a = 0.64$ m, $B_\phi = 1.3$ T) [35], JET ($R_0 = 3.0$ m, $a = 1.1$ m, $B_\phi = 3.0$ T) [1] and ITER ($R_0 \sim 6.0$ m, $a \sim 2.2$ m, $B_\phi \sim 4.9$ T) [51].

The discharge parameters chosen for this study are $q_\psi = 3.5$, $\bar{n}_e = 2 \times 10^{19}$ m⁻³, $\gamma = 0.5$, $\gamma_T = 2.0$, $M_{\text{eff}} = 2.0$, $Z_{\text{eff}} = 3.0$, $\kappa_X = 0.0$ (see Appendices A and B). In smaller tokamaks (e.g. COMPASS-C), these correspond to standard Ohmic operation in deuterium, at densities well below the density limit. In larger tokamaks, the parameters describe typical low density Ohmic ‘target plasmas’ used to access reactor-relevant plasma performance regimes via the addition of strong auxiliary heating (e.g. the DIII-D VH mode [52] and the JET trace tritium experiment [53]).

Figure 5 shows the hydrodynamic (τ_H), resistive (τ_R), viscous (τ_V) and neoclassical poloidal flow damping (τ_D)

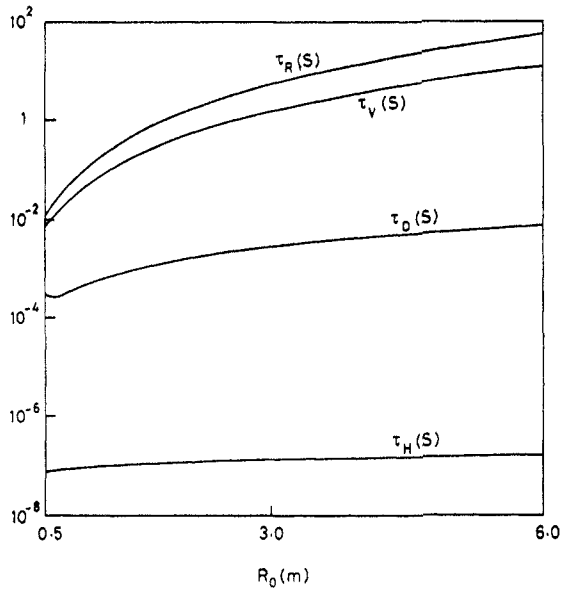


FIG. 5. Typical hydromagnetic (τ_H), resistive (τ_R), viscous (τ_V) and neoclassical poloidal flow damping (τ_D) time-scales for a (2, 1) mode, evaluated as functions of the major radius (R_0), using the scaling model for ohmically heated plasmas described in Appendix B. The minor radius is given by $a = 0.35R_0$, and the toroidal field strength by $B_\phi = 1.38R_0^{0.7}$ T. The discharge parameters are $q_\psi = 3.5$, $\bar{n}_e = 2 \times 10^{19} \text{ m}^{-3}$, $\gamma = 0.5$, $\gamma_T = 2.0$, $M_{\text{eff}} = 2.0$, $Z_{\text{eff}} = 3.0$ and $\kappa_X = 0.0$.

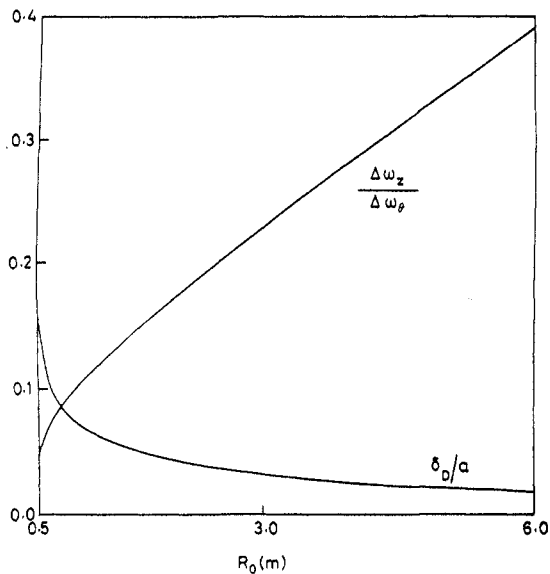


FIG. 6. Steady state localization scale length for the poloidal velocity shift profiles associated with, for example, locked modes as a fraction of the minor radius (δ_D/a), and the related ratio of 'toroidal' to poloidal mode frequency shifts ($\Delta\omega_z/\Delta\omega_p$), calculated as a function of the major radius (R_0) for the same set of parameters as those used in Fig. 5.

time-scales for a (2, 1) mode, evaluated as functions of the major radius R_0 , using the simple scaling model for ohmically heated plasmas described in Appendix B.

Figure 6 shows the steady state localization scale length for the poloidal velocity shift profiles associated with locked modes, for example (see Eqs (44a-d) and (161)), and the related ratio of toroidal to poloidal mode frequency shifts (see Eq. (162)), calculated for a (2, 1) mode using the neoclassical poloidal flow damping time-scale. It can be seen that the neoclassical time-scale yields increasingly strong localization of poloidal velocity shift profiles as R_0 increases, but that the degree of localization is insufficient to prevent the mode frequency shift from being mostly *poloidal* in nature (i.e. mostly due to changes in the poloidal, rather than the toroidal, component of the plasma velocity at the rational surface).

The latter prediction is completely at variance with experiment. For instance, a study in JET of the slowing down of mode rotation due to interaction with the vacuum vessel concludes that the associated plasma velocity change is predominantly in the *toroidal* direction [16, 54]. In COMPASS-C, a fairly comprehensive study of mode penetration comes to the conclusion that the plasma velocity change associated with the creation of a locked mode is also predominantly toroidal [29]. In DIII-D, independent spectroscopic measurements of the poloidal and toroidal ion velocities during the slowing down, and eventual penetration, of a mode interacting with a resonant external magnetic perturbation have confirmed that large changes are induced in the toroidal rotation, but that the poloidal rotation is little affected [55].

In fact, theory and experiment can only be reconciled if the poloidal damping time-scale is significant *smaller* than the neoclassical value. This conclusion is unlikely to be an artifact of the scaling model, or the ad hoc form adopted for the damping term in Eqs (25a, b), because the neoclassical damping time-scale falls so far short of that needed to account for the experimental observations.

One possible explanation for this apparent discrepancy is that the perpendicular viscosity is much larger in the poloidal direction than in the toroidal direction. Alternatively, poloidal flow damping may be dominated by collisionless processes (e.g. Landau damping) rather than the collisional processes considered in neoclassical theory. In the following, it is assumed that $\tau_D \rightarrow 0$, so that the plasma velocity changes due to locked modes, for example, are *entirely* toroidal. This assumption is generally found to be consistent with experimental observations.

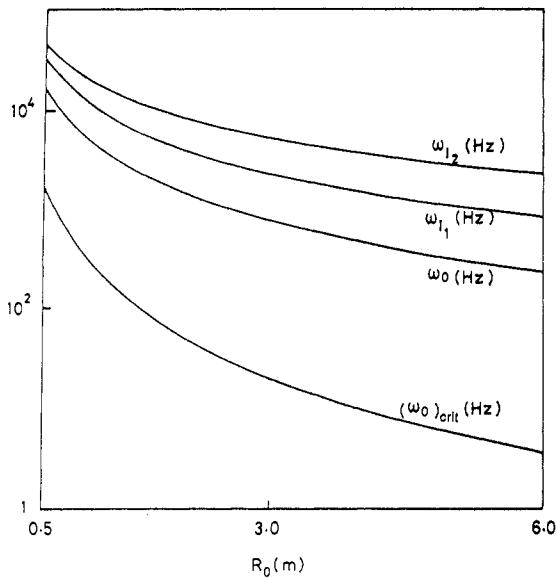


FIG. 7. The natural frequency (ω_0), the critical natural frequency [$(\omega_0)_{crit}$], the critical frequency mismatch above which a driven tearing layer becomes ideal (ω_{I_1}) and the critical frequency mismatch above which the layer becomes ideal inertial (ω_{I_2}), for a (2, 1) mode, calculated as functions of the major radius (R_0) for the same set of parameters as those used in Fig. 5.

Figure 7 shows the natural (2, 1) mode frequency (ω_0), the critical natural frequency ($(\omega_0)_{crit}$, see Section 7.4.3), the critical frequency mismatch above which a driven (2, 1) tearing layer becomes ideal ($\omega_{I_1} \equiv \tau_V^{1/3}/\tau_H^{2/3}\tau_R^{2/3}$, see Section 7.5) and the critical frequency mismatch above which the layer becomes ideal inertial ($\omega_{I_2} \equiv 1/\tau_H^{2/3}\tau_V^{1/3}$, see Section 7.5), as functions of the major radius. According to Fig. 7, in ohmically heated tokamaks the natural mode frequency ω_0 is considerably larger than the critical value $(\omega_0)_{crit}$, which is effectively the inverse layer reconnection time-scale. It follows from Section 7.4 that externally induced reconnection in a tearing-stable plasma (due to application of a static resonant magnetic perturbation, say) is highly discontinuous in nature. Below a critical perturbation field strength, there is some modification of the bulk toroidal plasma rotation, but relatively little magnetic reconnection is driven at the rational surface. As the critical field strength is exceeded, there is a sudden change in the plasma rotation as a large locked island is induced at the rational surface. This process is termed 'mode penetration' and is characterized by the absence of any rotating magnetic precursor to the locked mode.

Figures 5 and 7 suggest that, to a good approximation, $\tau_R \gg \tau_V$ and $\omega_0 \ll \omega_{I_1}$ for (2, 1) modes in ohmically heated tokamaks. It follows that mode penetration

lies in the visco-resistive limit described in Section 7.4, with the modification of plasma rotation prior to penetration governed by Eq. (124) and the penetration threshold itself given by Eq. (125).

For a non-tearing-stable plasma, the analogue of mode penetration is the mode locking mechanism discussed in Section 7.6. According to this, if the saturated island width exceeds the visco-resistive layer width δ_{layer} (see Fig. 8), then the modification of plasma rotation prior to mode locking is described by Eq. (137), and the locking threshold itself is given by Eq. (138). This locking mechanism is associated with periodic modulations in the island width as the rotating mode is alternatively stabilized and destabilized via interaction with the static magnetic perturbation. This is likely to be the dominant locking mechanism in ohmically heated tokamaks because the alternative locking mechanism, associated with periodic modulations in the island frequency as the rotating mode is alternatively speeded up and slowed down by the interaction (see Section 6), turns out to have an extremely high threshold.

Figure 8 shows the visco-resistive linear layer width $\delta_{layer} = 2.56(\tau_H^{1/3}/\tau_R^{1/6}\tau_V^{1/6})r_s$, the critical vacuum island width for visco-resistive mode penetration ($W_{pen,1}$, see Eq. (125)) and the critical vacuum island width for

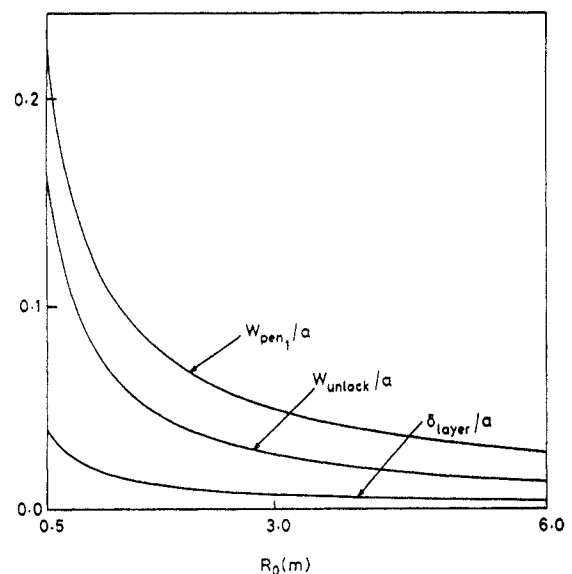


FIG. 8. The visco-resistive linear layer width divided by the minor radius (δ_{layer}/a), the critical vacuum island width for visco-resistive mode penetration divided by the minor radius ($W_{pen,1}/a$) and the critical vacuum island width for unlocking divided by the minor radius (W_{unlock}/a), for a (2, 1) mode, calculated as functions of the major radius (R_0) for the same set of parameters as those used in Fig. 5.

unlocking (W_{unlock} , see Eq. (74d)), calculated for (2, 1) modes, and expressed as a fraction of the minor radius. It can be seen that the layer width is quite substantial in small tokamaks, but falls rapidly with increasing machine size. The quantity W_{unlock} is, broadly speaking, the minimum locked island width that can be maintained in a tearing-stable plasma by a static external magnetic perturbation (see Section 5.4). In small tokamaks, where the natural mode frequency is comparatively high, only a very large locked island can be maintained against the strong viscous restoring torque acting in the plasma. As the machine dimensions increase, the natural frequency decreases and the restoring torque becomes progressively weaker, permitting ever smaller locked islands to be maintained in the plasma.

Figure 9 shows critical vacuum radial perturbation field strength at the plasma edge for (2, 1) visco-resistive mode penetration and unlocking, expressed as a fraction of the toroidal magnetic field strength. It can be seen that the critical magnetic perturbation amplitude needed to induce or maintain a locked mode decreases markedly with increasing machine size. Comparison with experimental data [29, 35, 36] reveals that the theoretical mode penetration threshold is about a factor of two too high, although it

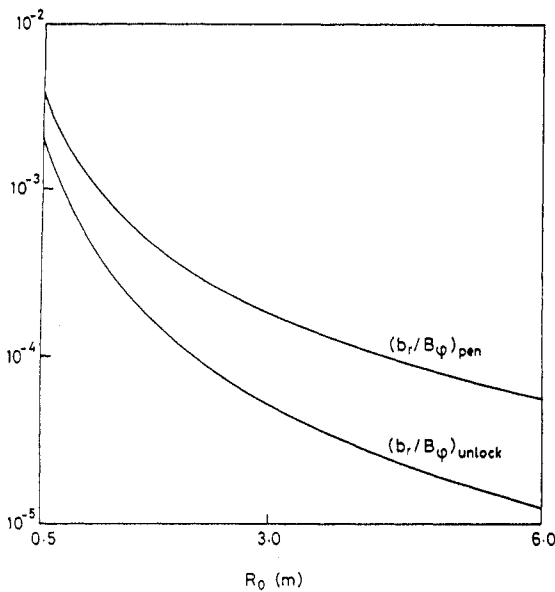


FIG. 9. The critical vacuum radial perturbation field strength at the plasma edge for visco-resistive mode penetration divided by the equilibrium toroidal field strength $((b_r/B_\phi)_{\text{pen}})$, and the critical field strength for unlocking divided by the toroidal field strength $((b_r/B_\phi)_{\text{unlock}})$, for a (2, 1) mode, calculated as functions of the major radius (R_0) for the same set of parameters as those used in Fig. 5.

predicts the relative scaling from machine to machine fairly accurately. This discrepancy could be due to shortcomings in the vacuum eigenfunction approximation used throughout this paper, or inaccuracies in the scaling model described in Appendix B (in particular in the scaling of the viscosity, which is not very well known). However, the most probable source of inaccuracy is the approximation of the suppressed island state as a linear layer employed in Section 7. The theory described in Refs [19] and [29], in which the suppressed island is treated as a fully non-linear island, actually gives better agreement with experiment for the penetration threshold, but is unable to account for the observed modification of plasma rotation prior to penetration.

Note that in small tokamaks, such as COMPASS-C, the critical perturbation strength required for penetration ($b_r/B_\phi > 10^{-3}$) is much larger than any conceivable field error. For medium to large tokamaks, such as DIII-D and JET, the critical perturbation strength ($b_r/B_\phi < 5 \times 10^{-4}$) is similar to the known level of field errors. In fact, field error induced (2, 1) mode penetration is observed in both devices at low density [35, 36] and can significantly restrict the disruption free operating space unless remedial action is taken (e.g. reducing the field errors [35] and 'spinning' the plasma with neutral beams [55]). For a tokamak of the (proposed) size of ITER, the critical perturbation strength for penetration ($b_r/B_\phi > 5 \times 10^{-5}$) is extremely low. Clearly, if ITER is to avoid the same (or worse!) problems with field error induced locked modes which have beset DIII-D, and to a lesser extent JET, the level of field errors will need to be kept significantly below those found, at present, on either of these devices.

One method for raising the penetration threshold, and thereby reducing the sensitivity of the discharge to error fields, is to 'spin' the plasma with unbalanced neutral beam injection (NBI). This increases the natural frequency ω_0 , but also tends to decrease $\omega_{I_1} \equiv \tau_V^{1/3}/\tau_H^{2/3} \tau_R^{2/3}$ (basically because τ_R is larger in the hotter beam heated plasma). In fact, in contrast to ohmically heated plasmas, ω_0 tends to exceed ω_{I_1} in NBI plasmas. It follows that mode penetration lies in the ideal limit described in Section 7.5, with the modification of plasma rotation prior to penetration governed by Eqs (126) or (129), and the penetration threshold itself given by Eq. (128). This implies that the critical perturbation field strength for penetration scales like $\delta B \propto \sqrt{|\omega_0|}$ in NBI discharges, instead of like $\delta B \propto |\omega_0|$ in Ohmic discharges. In fact, the empirical scaling obtained from NBI discharges in DIII-D is $\delta B \propto |\omega|^{0.4}$ [55].

In ohmically heated discharges, penetration occurs when the tearing frequency has been reduced to one half of its original value. In NBI discharges, on the other hand, penetration occurs when the tearing frequency has been reduced to a fixed value (i.e. $\omega'_0 \sim \omega_{I_i}$), which is usually only a small fraction of its original value. It follows that a more marked relative reduction in the tearing frequency is expected in NBI discharges than in Ohmic discharges. In fact, in Ohmic discharges the reduction in the tearing frequency just prior to penetration, inferred from magnetic and spectroscopic data, is about 30% of the original value [29]. In NBI discharges a much larger reduction of up to 70% of the original value is observed [55].

Figure 10 shows the resonant wall time constant $(\tau_w)_{res} \approx 2/|\omega_0|$ at which the drag on a rotating island is maximum, calculated for a (2, 1) mode (see Section 3.5). The critical island width for significant slowing down of island rotation due to interaction with a resonant wall is approximately W_{unlock} . It follows from Fig. 8 that in small tokamaks, even in the resonant case $\tau_w \sim (\tau_w)_{res}$, only extremely large islands can be slowed down by the wall. On the other hand, if the wall is resonant in ITER, then islands as small as 2% of the minor radius will be significantly slowed down. In this situation there will effectively be no conventional rotating MHD activity, since all substantial modes will be 'quasi-stationary' [54] owing to strong interaction with the wall.

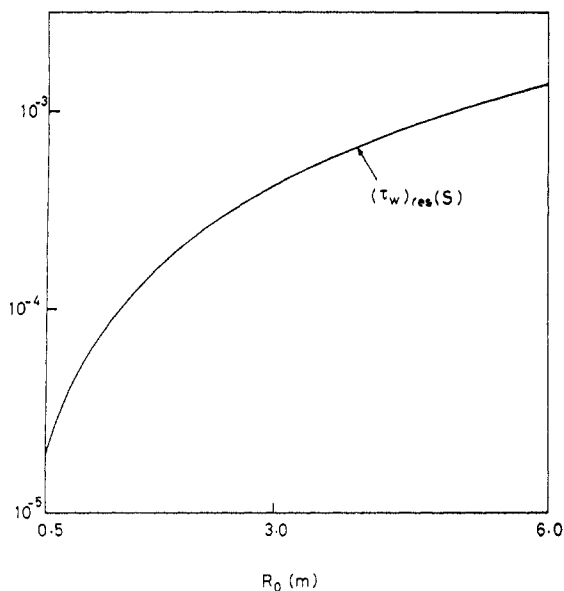


FIG. 10. The resonant wall time constant $[(\tau_w)_{res}]$ (in seconds) for a (2, 1) mode, calculated as a function of the major radius (R_0) for the same set of parameters as those used in Fig. 5.

This is clearly undesirable since it will facilitate mutual locking of the various modes in the plasma (which is destabilizing) and will also make it easier for the modes to lock to external field errors. It follows that some care must be taken during the design of ITER to ensure that the wall is significantly off resonance (i.e. τ_w is either much larger than, or much smaller than, $(\tau_w)_{res} \sim 1$ ms).

9. SUMMARY AND CONCLUSIONS

In Section 2 a basic theoretical framework is developed for the investigation of tearing mode interactions in cylindrical geometry. The problem is split into three main parts. In the first part, the marginally stable ideal MHD equations are solved in the region of the plasma where ideal MHD holds, subject to suitable boundary conditions. This enables the stability of the various modes in the plasma to be assessed and also allows the electromagnetic torques acting in the plasma to be evaluated. In the second part, fluid equations describing modifications to the bulk plasma rotation are solved in the ideal MHD region of the plasma, subject to suitable boundary conditions. This enables the viscous torques acting in the plasma to be evaluated. In the final part, the electromagnetic and fluid components of the model are combined to give a set of equations describing the coupled evolution of the *amplitude* and *phase* of each mode in the plasma.

The scheme outlined above is, of course, much more involved than the standard non-interacting tearing mode problem. This is due to the fact that there is, in general, more than one frequency in the system. For instance, for the case of many interacting tearing modes resonant on different rational surfaces in the plasma, each mode will have its own preferred rotation frequency (the so called 'natural' frequency). In general, there is very little response if a tearing mode is driven off resonance (i.e. at a frequency substantially different from its natural frequency) [19]. However, the frequency of each mode in the plasma can be non-linearly modified by the electromagnetic torques acting in the vicinity of the various rational surfaces. These torques act to bring all modes into co-rotation, where the mutual interaction is at a maximum. Such frequency modifications are opposed by viscous restoring torques. It follows that the stability of the various modes in the plasma is a strong function of the tearing frequencies at each rational surface, which in turn depend on the relative strengths of the electromagnetic and viscous torques. Of course, these torques are sensitive functions of the

amplitudes, phases and rotation frequencies of the various modes in the plasma. Thus, a highly non-linear set of equations is obtained, which can lead to a rich variety of different types of behaviour, even for apparently quite simple systems. The interaction of a tearing mode with a static external structure (e.g. an error field) is similar in form to the coupled tearing mode problem, except that one of the frequencies in the system (i.e. that corresponding to the external structure) is always zero.

In Section 3 the slowing down of a rotating magnetic island interacting with a resistive wall is investigated, and the results are summarized in Section 3.5. The main result is that for a sufficiently large unperturbed island rotation frequency there is a bifurcation of steady state solutions, so that if the interaction strength exceeds a certain critical value there is a sudden decrease in the island rotation to a very small value, accompanied by a sudden change in the bulk plasma rotation.

In Sections 4–7 the interaction of a tearing mode with a static resonant magnetic perturbation is investigated. Five distinct types of interaction are found. **Mode unlocking** is the transition from a locked island state to a rotating island state, and takes place when the perturbation strength falls below a critical value. **Mode locking** is the inverse process, and can take place via predominantly viscous, inertial or resistive mechanisms, if the perturbation strength is sufficiently large. The slightly non-uniform rotation of a non-locked magnetic island interacting with a static magnetic perturbation gives rise to a net *stabilizing* effect on the mode, in marked contrast to a locked island where the interaction is always *destabilizing*. **Mode stabilization** can take place via predominantly viscous or inertial mechanisms. A sufficiently small saturated island can be completely stabilized, but if the island is too large then locking occurs prior to complete stabilization. The interaction of a tearing-stable plasma with a static magnetic perturbation can give rise to modification of the bulk plasma rotation. This process is known as **plasma rotation braking** and takes place without any substantial magnetic reconnection being driven at the rational surface. However, if the perturbation strength exceeds a critical value there is a large change in the plasma rotation, as a locked island is induced at the rational surface. This process is known as **mode penetration**, and is distinguished from conventional mode locking by the absence of any rotating magnetic precursor to the locked island. All of the above mentioned effects are observed in experiment.

In Section 8, some of the results derived in Sections 3–7 are applied to typical ohmically heated

tokamak discharges with the aid of the simple scaling model described in Appendix B. The neoclassical poloidal flow damping time-scale is found to be significantly too large to account for the experimental observation/inference that mode frequency shifts induced by resistive walls or static magnetic perturbations are predominantly due to toroidal, rather than poloidal, velocity shifts at the rational surface. The mode penetration threshold is found to decrease rapidly with increasing machine size, placing stringent limits on the permissible error field level in ITER if problems with locked modes are to be avoided. Finally, it is pointed out that a certain range of values for the wall time constant in ITER will lead to the collapse of MHD rotation at extremely small saturated amplitudes. Since this is clearly undesirable, it is important that this range of values be avoided.

The most important conclusion of this paper is that application of an (m, n) magnetic perturbation does not necessarily give rise to driven reconnection at the (m, n) mode rational surface(s) in the plasma [19]. In fact, unless the perturbation rotates at the natural frequency of the plasma (m, n) mode, no substantial reconnection is driven until a certain threshold perturbation strength is exceeded. This threshold strength is basically that required to shift the (m, n) tearing frequency off its natural value, such that it becomes coincident with the applied frequency. Although this conclusion is deduced from a study of the interaction of a single tearing mode with an external perturbation, it is also likely to hold for toroidal coupled tearing modes.

The results derived in Sections 4–7 suggest that a magnetic island on a particular rational surface which is not of sufficient amplitude to lock neighbouring (i.e. toroidally coupled) rational surfaces actually has a *stabilizing* effect on modes resonant on these surfaces. Also the Δ' of the low amplitude mode should, to a first approximation, be worked out using an eigenfunction which behaves *ideally* (i.e. with zero reconnection) at the neighbouring surfaces. As the island grows, it will eventually reach sufficient amplitude to lock one of the neighbouring rational surfaces, at which point a co-rotating island will be induced at this surface, and the original mode will become more unstable. Note that the co-rotating island will not, in general, be exactly in phase with the original island, owing to the viscous torques acting in the plasma. There will be a change in the bulk plasma rotation associated with the locking of a neighbouring rational surface, tending to bring the tearing frequencies of the various modes in the plasma closer together. Further growth of the island may lock the other neighbouring surfaces, one by one, or may lead to catastrophic

locking of all the surfaces. Note that the more surfaces a given island is able to lock, the more unstable it is likely to become.

In conclusion, the study of tearing mode interactions in cylindrical geometry has given rise to many rewarding insights into tearing mode behaviour. It is hoped that it will be possible, in the not too distant future, to complete a complementary study of tearing mode interactions in toroidal geometry.

Appendix A

THE SCRAPE-OFF LAYER

The boundary condition satisfied by the perturbed velocity at the edge of the plasma is parametrized by κ_X (see Eqs (28a, b)). In this appendix, a simple model of the scrape-off layer is developed that enables κ_X to be estimated from the edge plasma parameters.

Consider a scrape-off layer produced by a single poloidal ring limiter, extending from $r = a$ (the radius of the last closed flux surface) to $r = a + d$ (the radius of the vacuum vessel). For the sake of simplicity, the scrape-off layer is assumed to be uniform in the poloidal and toroidal directions. The angular momentum of the ion fluid is gradually destroyed as the individual ions collide with the limiter. The rate of destruction of angular momentum is approximately v_{thi}/L_c , where v_{thi} is the ion thermal velocity (i.e. the velocity with which ions stream along field lines) and $L_c \approx 2\pi R_0$ is the connection length along field lines from one side of the limiter to the other.

The destruction of fluid angular momentum via collisions with the limiter can be incorporated into Eqs (25a, b), yielding a simple one dimensional equation describing the perturbed 'toroidal' flow in the scrape-off layer. Thus,

$$\rho(a) \frac{\partial \Delta \Omega_z}{\partial t} \approx \mu_{\perp}(a) \frac{\partial^2 \Delta \Omega_z}{\partial x^2} - \rho(a) \frac{v_{thi}}{2\pi R_0} \Delta \Omega_z \quad (140)$$

where $x = r - a$. Here, the scrape-off layer is assumed to be thin compared with the plasma cross-section, and any variations in the density and viscosity across the layer are neglected. The steady state solution of Eq. (140) that satisfies the physical boundary condition imposed at the wall, $\Delta \Omega_z(a + d) = 0$, is

$$\Delta \Omega_z(r) = \Delta \Omega_z(a) \frac{\sinh[(a + d - r)/\lambda_{sol}]}{\sinh(d/\lambda_{sol})} \quad (141)$$

for $r \geq a$, where

$$\lambda_{sol} = \left(\frac{\mu_{\perp}(a) 2\pi R_0}{\rho(a) v_{thi}} \right)^{1/2} \quad (142)$$

Equation (141) yields

$$\kappa_X \equiv -\Delta \Omega_z(a) \left/ a \frac{\partial \Delta \Omega_z(a)}{\partial r} \right. = \frac{\lambda_{sol}}{a} \tanh\left(\frac{d}{\lambda_{sol}}\right) \quad (143)$$

(see Eqs (28a, b)).

It is easily demonstrated that the fraction of the 'toroidal' viscous torque transmitted to the scrape-off layer by the bulk plasma that develops on the wall is

$$\frac{T_{z \text{ wall}}}{T_{z \text{ sol}}} = \frac{1}{\cosh(d/\lambda_{sol})} \quad (144)$$

The remainder of the torque transmitted to the scrape-off layer ends up on the limiter. Note that in a steady state the total 'toroidal' torque that develops on the wall and limiter is equal to the total 'toroidal' electromagnetic torque acting inside the plasma (see Eqs (32a, b)).

The boundary condition, $\Delta \Omega_z(a + d) = 0$, can be justified by modelling the wall as a set of closely spaced poloidal ring limiters. In the limit where the spacing goes to zero, the above analysis yields $L_c \rightarrow 0$, $\lambda_{sol} \rightarrow 0$, $\kappa_X \rightarrow 0$, and hence $\Delta \Omega_z \rightarrow 0$, at the wall.

Equations (143) and (144) imply that if the velocity decay scale length in the scrape-off layer λ_{sol} is much smaller than the maximum width of the layer d , then $\kappa_X \approx \lambda_{sol}/a$ and nearly all of the torque transmitted to the layer ends up on the limiter. On the other hand, if λ_{sol} is much greater than d , then $\kappa_X \approx d/a$ and nearly all of the torque transmitted to the layer ends up on the wall. Thus, the maximum possible value of κ_X is d/a . Now, in most tokamaks the radial extent of the limiter is only a small fraction of the plasma radius. It follows that κ_X is always much smaller than unity. Any process, such as charge exchange with neutrals [44], which gives rise to additional edge plasma momentum losses, will tend to reduce κ_X still further.

Appendix B

A SCALING MODEL FOR OHMICALLY HEATED TOKAMAKS

The vacuum safety factor profile

$$q = q_{\psi} x^2 \quad (145)$$

is adopted for consistency with the vacuum eigenfunctions employed in Sections 3 and 4 (see Eqs (36a-c) and (61a, b)). Here, q_{ψ} is the edge safety factor and $x = r/a$. The magnetic shear associated with the

vacuum q profile is $s \equiv rq'/q = 2$. The rational surface is located at $r_s/a = \sqrt{q_s/q_\psi}$. The density and temperature profiles are assumed to take the form

$$n_e(x) = G(\gamma)\bar{n}_e(1 - x^2)^\gamma \quad (146a)$$

$$T_{(i,e)}(x) = T_{(i,e)}(1 - x^2)^{\gamma\tau} \quad (146b)$$

where n_e is the electron number density, \bar{n}_e the line averaged electron number density, T_e the electron temperature, T_i the ion temperature and

$$G(\gamma) = \frac{2}{\sqrt{\pi}} \frac{\Gamma(\gamma + \frac{3}{2})}{\Gamma(\gamma + 1)} \quad (147)$$

The central electron temperature is estimated by balancing the volume averaged Ohmic heating power, calculated using the classical parallel resistivity [41, 56]

$$\eta_{\parallel}(\Omega \cdot \text{m}) = 1.65 \times 10^{-9} \frac{Z_{\text{eff}} \ln \Lambda_e}{T_e(\text{keV})^{3/2}} \quad (148)$$

against the volume averaged rate of electron energy losses, calculated using the neo-Alcator energy confinement time-scale [57]

$$\tau_E(\text{s}) = 7 \times 10^{-3} \bar{n}_e(10^{19} \text{ m}^{-3}) a(\text{m}) R_0^2(\text{m}) q_\psi \quad (149)$$

yielding

$$T_e(\text{keV}) = 0.20 \left(\frac{B_\phi^2(\text{T}) a(\text{m})}{q_\psi} Z_{\text{eff}} \ln \Lambda_e \times \frac{(1 + \frac{3}{2}\gamma\tau)(1 + \gamma + \gamma\tau)}{G(\gamma)} \right)^{2/5} \quad (150)$$

Here, a is the plasma minor radius, R_0 the major radius of the magnetic axis, B_ϕ the toroidal magnetic field strength and Z_{eff} the effective charge number of the ions. The volume averaged Coulomb logarithm for electron-ion collisions is given by (see Ref. [56])

$$\ln \Lambda_e = 16.4 - \frac{1}{2} \ln \bar{n}_e(10^{19} \text{ m}^{-3}) + \ln T_e(\text{keV}) - \ln(1 + \gamma\tau) \quad (151)$$

The neoclassical enhancement of plasma resistivity [56] is neglected in Eq. (148) for the sake of simplicity. It can be crudely simulated by increasing Z_{eff} by an appropriate factor. The neo-Alcator scaling of τ_E is valid for most ohmically heated tokamak plasmas, except at high densities (above $\bar{n}_e \sim 8 \times 10^{19} \text{ m}^{-3}$, say [58]) where the confinement 'saturates' (i.e. τ_E ceases to increase with density).

The central ion temperature is evaluated by balancing the volume averaged rate of heating by the electrons, calculated using the classical electron-ion energy exchange time-scale [41]

$$\tau_{\text{ex}}(\text{s}) = 0.67 \frac{M_{\text{eff}} T_e^{3/2}(\text{keV})}{Z_{\text{eff}} \ln \Lambda_e G(\gamma) \bar{n}_e(10^{19} \text{ m}^{-3})} \quad (152)$$

against the volume averaged rate of ion energy losses, calculated using the neo-Alcator energy confinement time-scale, yielding

$$\frac{T_{i,c}}{T_e} = \left(1 + \frac{\tau_{\text{ex}}(1 + 2\gamma - \gamma\tau/2)}{\tau_E(1 + \gamma + \gamma\tau)} \right)^{-1} \quad (153)$$

In Eq. (152), M_{eff} is the effective mass number of the ions (in units of the proton mass). Note that the electron and ion energy confinement time-scales have been assumed to be equal, for the sake of simplicity.

Neglecting profile effects, the viscosity time-scale τ_V (defined in Eq. (52g)) is related to the momentum confinement time-scale τ_M (i.e. the time-asymptotic e-folding time for the viscous decay of an *unsupported* 'toroidal' velocity shift profile) via (see Ref. [29])

$$\tau_V = 5.78 \left(\frac{q_s}{q_\psi} \right) \tau_M \quad (154)$$

The momentum confinement time-scale τ_M is set equal to the neo-Alcator energy confinement time-scale (149), evaluated at a fixed density ($\bar{n}_e \sim 2 \times 10^{19} \text{ m}^{-3}$, say). This is reasonable, since τ_M is observed to be similar in magnitude to τ_E in most tokamaks [59]. The comparative lack of variation of τ_M with plasma density (in low density ohmically heated tokamaks) is consistent with the observed rate of increase of the penetration threshold for static external magnetic perturbations with increasing density [29, 35, 36].

The hydromagnetic and resistive time-scales (defined in Eqs (52f) and (21)) take the form

$$\tau_H(\text{s}) = 7.2 \times 10^{-8} \frac{R_0(\text{m})}{nB_\phi(\text{T})} [M_{\text{eff}} G(\gamma) \bar{n}_e(10^{19} \text{ m}^{-3})]^{1/2} \times (1 - q_s/q_\psi)^{\gamma/2} \quad (155a)$$

$$\tau_R(\text{s}) = 7.6 \times 10^2 \frac{a^2(\text{m}) T_e^{3/2}(\text{keV})}{Z_{\text{eff}} \ln \Lambda_e} \times \frac{q_s}{q_\psi} \left(1 - \frac{q_s}{q_\psi} \right)^{3\gamma\tau/2} \quad (155b)$$

The natural mode (angular) frequency ω_0 is set equal to the electron diamagnetic frequency, so that

$$\omega_0(\text{rad} \cdot \text{s}^{-1}) = 2m \frac{T_e(\text{keV})}{a^2(\text{m}) B_\phi(\text{T})} (\gamma + \gamma\tau) \times (1 - q_s/q_\psi)^{\gamma\tau-1} \quad (156)$$

As is demonstrated in Ref. [7], this is an extremely good scaling law for ohmically heated tokamaks.

According to standard neoclassical theory, poloidal flow damping in tokamaks is due to magnetic pumping in the Pfirsch-Schlüter regime [42] and friction between

trapped and passing ions in the banana regime [60]. A somewhat simplified formula for the poloidal flow-damping time-scale τ_D at the rational surface can be derived from the neoclassical formalism of Ref. [60]. Thus,

$$\tau_D \approx 1.29 \frac{\tau_{ii}}{\sqrt{\epsilon_s}} \left(1 + \frac{0.19}{\epsilon_s^{3/2} \lambda_i^2} \right) \quad (157)$$

where $\epsilon_s = (q_s/q_\psi)^{1/4} \sqrt{a/R_0}$,

$$\tau_{ii} \text{ (s)} = 4.7 \times 10^{-2} \frac{M_{\text{eff}}^{1/2} T_i^{3/2} \text{ (keV)}}{G(\gamma) \bar{n}_e (10^{19} \text{ m}^{-3}) \ln \Lambda_i} \times \frac{(1 - q_s/q_\psi)^{3\gamma\tau/2}}{(1 - q_s/q_\psi)^\gamma} \quad (158)$$

is the classical ion-ion collision time-scale, and

$$\lambda_i \equiv \tau_{ii} \omega_{tr_i} = 2.1 \times 10^4 \frac{T_i^{5/2} \text{ (keV)}}{G(\gamma) \bar{n}_e (10^{19} \text{ m}^{-3}) \ln \Lambda_i R_0 \text{ (m)} q_s} \times \frac{(1 - q_s/q_\psi)^{5\gamma\tau/2}}{(1 - q_s/q_\psi)^\gamma} \quad (159)$$

parametrizes the ion collisionality. Here, ω_{tr_i} is the ion transit frequency around the rational flux surface. The volume averaged Coulomb logarithm for ion-ion collisions takes the form

$$\ln \Lambda_i = 18.5 - \frac{1}{2} \ln \bar{n}_e (10^{19} \text{ m}^{-3}) + \frac{3}{2} \ln T_i \text{ (keV)} - \frac{3}{2} \ln (1 + \gamma_T) \quad (160)$$

[56]. Equation (157) yields the correct asymptotic formula for τ_D in both the Pfirsch-Schlüter ($\lambda_i \rightarrow 0$) and the banana ($\lambda_i \rightarrow \infty$) limits. The effect of impurities has been neglected for the sake of simplicity. In fact, it can be demonstrated that under normal circumstances impurities only give rise to an $O(1)$ correction to τ_D .

The steady state localization scale length for the poloidal velocity shift profiles associated with, for example, locked modes is given by

$$\frac{\delta_D}{a} = \sqrt{\frac{q_s \tau_D}{q_\psi \tau_V}} \quad (161)$$

(see Eq. (45) and Section 3.4.3). The related ratio of the mode frequency shift attributable to changes in the poloidal velocity at the rational surface, $\Delta\omega_\theta = m\Delta\Omega_{\theta s}$, to the frequency shift attributable to changes in the 'toroidal' velocity, $\Delta\omega_z = -n\Delta\Omega_{zs}$, is

$$\frac{\Delta\omega_\theta}{\Delta\omega_z} = \frac{1}{2} \sqrt{\frac{\tau_D}{\tau_V} \frac{q_s q_\psi}{(a/R_0)^2}} \left(\frac{1}{2} \ln (q_\psi/q_s) + \kappa_X \right) \quad (162)$$

in steady state (see Eq. (50)). Here, any variation of $\mu_\perp(r)$ with r has been neglected.

ACKNOWLEDGEMENTS

The author would like to thank J.A. Wesson (JET) whose ideas, many of which remain unpublished, form the basis for much of this paper. The author would also like to thank J. Hugill (Culham) and Professor M.G. Haines (Imperial College, London) for many enlightening discussions regarding plasma rotation.

This research was jointly funded by the UK Department of Trade and Industry and by Euratom.

REFERENCES

- [1] WESSON, J.A., et al., Nucl. Fusion **29** (1989) 641.
- [2] McGUIRE, K.M., et al., Plasma Phys. Control. Fusion **30** (1988) 1391.
- [3] WESSON, J.A., Nucl. Fusion **18** (1978) 87.
- [4] FURTH, H.P., et al., Phys. Fluids **6** (1963) 459.
- [5] RUTHERFORD, P.H., Phys. Fluids **16** (1973) 1903.
- [6] BUSSAC, M.N., et al., in Plasma Physics and Controlled Nuclear Fusion Research 1976 (Proc. 6th Int. Conf. Berchtesgaden, 1976), Vol. 1, IAEA, Vienna (1977) 607.
- [7] CHEN, Y.J., et al., in Research Using Small Tokamaks (Proc. Tech. Comm. Mtg Arlington, 1990), IAEA, Vienna (1990) 41.
- [8] STORK, D., et al., in Controlled Fusion and Plasma Physics (Proc. 14th Eur. Conf. Madrid, 1987), Vol. 11D, Part I, European Physical Society, Geneva (1987) 306.
- [9] BONDESON, A., IACONO, R., in Theory of Fusion Plasmas (Proc. Varenna-Lausanne Int. Workshop Chexbres, 1988), Editrice Compositori, Bologna (1989) 57.
- [10] BOOZER, A.H., Phys. Fluids **24** (1981) 1387.
- [11] JENSEN, T.H., CHU, M.S., J. Plasma Phys. **30** (1983) 57.
- [12] RUTHERFORD, P.H., in Basic Physical Processes of Toroidal Fusion Plasmas (Proc. Course and Workshop Varenna, 1985), Vol. 2, CEC, Brussels (1986) 531.
- [13] PERSSON, M., BONDESON, A., Nucl. Fusion **29** (1989) 989.
- [14] HENDER, T.C., et al., Nucl. Fusion **29** (1989) 1279.
- [15] BERGE, G., et al., Phys. Scr. **40** (1989) 173.
- [16] NAVE, M.F.F., WESSON, J.A., Nucl. Fusion **30** (1990) 2575.
- [17] EDERY, D., SAMAIN, A., Plasma Phys. Control. Fusion **32** (1990) 93.
- [18] ZOHM, H., et al., Europhys. Lett. **11** (1990) 745.
- [19] FITZPATRICK, R., HENDER, T.C., Phys. Fluids B **3** (1991) 644.
- [20] HENDER, T.C., et al., in Controlled Fusion and Plasma Heating (Proc. 15th Eur. Conf. Dubrovnik, 1988), Vol. 12B, Part I, European Physical Society, Geneva (1988) 1367.
- [21] JENSEN, T.H., et al., Phys. Fluids B **3** (1991) 1650.
- [22] FITZPATRICK, R., et al., in Avoidance and Control of Disruptions in Tokamaks (Proc. Tech. Comm. Mtg Culham, 1991), IAEA, Vienna (1992) 100.
- [23] FITZPATRICK, R., et al., Bull. Am. Phys. Soc. **36** (1991) 2357.

FITZPATRICK

- [24] KURITA, G., TUDA, T., in *Advances in Simulation and Modelling of Thermonuclear Plasmas* (Proc. Tech. Comm. Mtg Montreal, 1992), IAEA, Vienna (in press).
- [25] PARKER, R.D., in *1992 International Conference on Plasma Physics* (Proc. Conf. Innsbruck, 1992), Vol. 16C, Part I, European Physical Society, Geneva (1992) 427.
- [26] KAGER, F., et al., in *Plasma Physics and Controlled Nuclear Fusion Research 1974* (Proc. 5th Int. Conf. Tokyo, 1974), Vol. 1, IAEA, Vienna (1975) 207.
- [27] BOL, K., et al., *ibid.*, 83.
- [28] ELLIS, J.J., et al., in *Plasma Physics and Controlled Nuclear Fusion Research 1984* (Proc. 10th Int. Conf. London, 1984), Vol. 1, IAEA, Vienna (1985) 363.
- [29] HENDER, T.C., et al., *Nucl. Fusion* **32** (1992) 2091.
- [30] McCOOL, S.C., et al., *Nucl. Fusion* **29** (1989) 547.
- [31] LEONARD, A.W., et al., *Nucl. Fusion* **31** (1991) 1511.
- [32] VALLET, J.C., et al., *Stabilization of Tokamak Discharges at the Density Limit by Means of the Ergodic Limiter*, Cadarache Rep. EUR-CEA-FC-1427, Association Euratom-CEA, Saint-Paul-lez-Durance (1991).
- [33] LaHAYE, R.J., SCOVILLE, J.T., *Rev. Sci. Instrum.* **62** (1991) 2146.
- [34] EVANS, T.E., in *Controlled Fusion and Plasma Physics* (Proc. 18th Eur. Conf. Berlin, 1991), Vol. 15C, Part II, European Physical Society, Geneva (1991) 65.
- [35] SCOVILLE, J.T., et al., *Nucl. Fusion* **31** (1991) 875.
- [36] FISHPOOL, G.M., et al., in *Avoidance and Control of Disruptions in Tokamaks* (Proc. Tech. Comm. Mtg Culham, 1991), IAEA, Vienna (1992) 84.
- [37] PERSSON, M., BONDESON, A., *Phys. Fluids B* **2** (1990) 2315.
- [38] PERSSON, M., *Nucl. Fusion* **31** (1991) 382.
- [39] ARA, G., et al., *Ann. Phys. NY* **112** (1978) 443.
- [40] VAHALA, G., et al., *Nucl. Fusion* **20** (1980) 17.
- [41] BRAGINSKII, S.I., in *Reviews of Plasma Physics*, Vol. 1 (LEONTOVICH, M.A., Ed.), Consultants Bureau, New York (1965) 205.
- [42] STIX, T.H., *Phys. Fluids* **16** (1973) 1260.
- [43] HAINES, M.G., *Adv. Phys.* **14** (1965) 167.
- [44] BRAU, K., et al., *Nucl. Fusion* **23** (1983) 1643.
- [45] WHITE, R.B., et al., *Phys. Fluids* **20** (1977) 800.
- [46] GIMBLETT, C.G., *Nucl. Fusion* **26** (1986) 617.
- [47] SOMETANI, T., FUKAGAWA, K., *Jpn. J. Appl. Phys.* **17** (1978) 2035.
- [48] LEE, J.K., et al., *Nucl. Fusion* **23** (1983) 63.
- [49] REIMAN, A., MONTICELLO, D., *Phys. Fluids B* **3** (1991) 2230.
- [50] HENDER, T.C., et al., in *Plasma Physics and Controlled Nuclear Fusion Research 1988* (Proc. 12th Int. Conf. Nice, 1988), Vol. 1, IAEA, Vienna (1989) 445.
- [51] ITER: Design Overview, *Plasma Physics and Controlled Nuclear Fusion Research 1990* (Proc. 13th Int. Conf. Washington, DC, 1990), Vol. 3, IAEA, Vienna (1991) 225.
- [52] JACKSON, G.L., et al., *Phys. Fluids B* **4** (1992) 2181.
- [53] JET TEAM, *Nucl. Fusion* **32** (1992) 187.
- [54] SNIPES, J.A., et al., *Nucl. Fusion* **28** (1988) 1085.
- [55] LaHAYE, R.J., et al., in *1992 International Conference on Plasma Physics* (Proc. Conf. Innsbruck, 1992), Vol. 16C, Part I, European Physical Society, Geneva (1992) 187.
- [56] WESSON, J.A., *Tokamaks*, Oxford Engineering Science Series, Vol. 20, Oxford University Press (1987).
- [57] PFEIFFER, W.W., WALTZ, R.E., *Nucl. Fusion* **19** (1979) 51.
- [58] CAROLAN, P.G., et al., in *Controlled Fusion and Plasma Physics* (Proc. 18th Eur. Conf. Berlin, 1991), Vol. 15C, Part I, European Physical Society, Geneva (1991) 81.
- [59] POST, D.E., et al., in *ITER Physics*, ITER Documentation Series, No. 21, IAEA, Vienna (1991).
- [60] KIM, Y.B., et al., *Phys. Fluids B* **3** (1991) 2050.

(Manuscript received 19 October 1992
Final manuscript received 23 April 1993)